A Dissertation

entitled

Simulating Microbial Enzyme Allocation During Plant Litter Decay in Response to Litter Lignin Content and C:N Stoichiometry

by

Michaela G. Margida

Submitted to the Graduate Faculty as partial fulfillment of the requirements for the

Doctor of Philosophy Degree in

Biology

_____

Dr. Daryl L. Moorhead, Committee Chair

_____

Dr. Jonathan M. Bossenbroek, Committee Member

_____

Dr. Gwenaëlle Lashermes, Committee Member

_____

Dr. Michael N. Weintraub, Committee Member

_____

Dr. Robert L. Sinsabaugh, Committee Member

_____

Dr. Amy Thompson, Acting Dean
College of Graduate Studies

The University of Toledo
August 2021

An Abstract of

Simulating Microbial Enzyme Allocation During Plant Litter Decay in Response to Litter Lignin Content and C:N Stoichiometry

by

Michaela G. Margida

Submitted to the Graduate Faculty as partial fulfillment of the requirements for the Doctor of Philosophy Degree in
Biology

The University of Toledo
August 2021

Herein we developed two mathematical models of microbial enzyme-driven, plant litter decomposition: (1) a two-substrate cellulose (C_2) and lignin (C_3) model including cellulolytic (E_2) and ligninolytic enzymes (E_3) and (2) a three-substrate organic nitrogen (C_1), cellulose (C_2), and lignin (C_3) model including nitrogen-acquiring (E_1), cellulolytic (E_2), and ligninolytic (E_3) enzymes. For the lignocellulose model, we set observed first-order decay rates equal to reverse Michaelis-Menten (RMM) equations to estimate relative enzyme activities associated with observed patterns of hollocellulose (C_2) and lignin (C_3) decay. Results were consistent with empirical studies, showing a negative relationship of $E_2/(E_2+E_3)$ to litter lignin content, $C_3/(C_2+C_3)$, above a minimum threshold of 40% lignin, at which lignin begins to decay. For the three-pool model, we solved for the allocation of each enzyme pool as functions of litter lignocellulose index (LCI), microbial and litter C:N stoichiometry, and constraints on total enzyme production, again setting observed decay rates equal to RMM equations. To our knowledge, the lignocellulose model is the first mechanistic explanation of microbial allocation of cellulolytic and ligninolytic enzymes as a function of the lignin

concentration of the lignocellulose complex. It was consistent with observations but raised questions about factors controlling the threshold for lignin decay. The three-pool model provides the first practical solution for analytically allocating microbial C- and N-acquiring enzymes as functions of both litter C-quality and C:N stoichiometry but insufficient data exist to reconcile these underlying controls with observed patterns of enzyme allocation and C and N dynamics during long-term litter decay.

For EvB, who has been written in my stars since long before we met. Wil je met me trouwen?

Acknowledgements

I thank Daryl L. Moorhead for his wise counsel, without which neither this dissertation, nor I, would exist in the current form. I thank Jonathan M. Bossenbroek for holding me accountable for communicating my research clearly beyond my immediate circle. I thank Gwenaëlle Lashermes for her co-authorship, especially her fine eye for detail and the provision of thoughtful and nuanced feedback. I thank Michael N. Weintraub for input during model development and for the excellent soil ecology course. I thank Robert L. Sinsabaugh for providing data used for model validation and for feedback that greatly improved the manuscript. I thank my fellow graduate students, especially Jessica Sherman Collier, for providing encouragement. I thank my parents, Andrea and Anthony Margida, and my brother, Gregory Margida, for supporting me in countless ways throughout my PhD journey. Finally, I thank my forever, Esther van Batenburg, for giving me the final push I needed to finish what I started. This research was supported in part by a University Research Funding Opportunities (URFO) Grant from the University of Toledo, and by the program grant 'scientific challenge' (FungiBioD) from the Environment and Agronomy Division of the National Institute of Agronomic Research (INRA), France.

Table of Contents

Abstract iii

Dedication v

Acknowledgements vi

Table of Contents vii

List of Tables x

List of Figures xi

1 Estimating Relative Cellulolytic and Ligninolytic Enzyme Activities as Functions of Lignin and Cellulose Content in Decomposing Plant Litter 1

1.1 Introduction 2

1.2 Modeling methods 5

1.2.1 Rationale 5

1.2.2 Validation 8

1.3 Results ……. 10

1.4 Discussion ……. 14

2 Estimating Eco-enzymatic Activities as a Function of Carbon Quality and Carbon-Nitrogen Stoichiometry During Plant Litter Decomposition 17

2.1 Introduction 19

2.1.1 Carbon-nitrogen stoichiometry 20

2.1.2 Carbon quality 22

2.1.3 Empirical evidence 23
2.1.4 Objectives 24
2.2 Modeling methods 25
2.2.1 Empirical data and observations 26
2.2.2 Modeling rationale 28
2.2.3 Carbon- and nitrogen- acquiring enzyme allocation 31
2.2.4 LCI controls 32
2.2.5 E_T controls 33
2.2.6 Balancing C and N fluxes 35
2.2.7 Carbon use efficiency 37
2.2.8 Sensitivity analysis 38
2.3 Results ……. 39
2.3.1 Litter and enzyme pools 39
2.3.2 General model behavior 41
2.3.3 Sensitivity analysis 45
2.3.4 Carbon use efficiency 47
2.4 Discussion ……. 48
2.4.1 Patterns of litter decay 48
2.4.2 Patterns of enzyme activities 51
2.4.3 Coupled C and N fluxes 54
2.4.4 Sensitivity analysis 55
2.4.5 Carbon use efficiency 57
2.4.6 Limitations and future directions 59

2.5 Conclusions……..... 60

References 62

A Chapter 2 Equations..... 76

List of Tables

1.1 Parameters used in modelling cellulolytic and ligninolytic enzyme allocations. ... 6

2.1 Linear equations used to estimate model drivers. 27

2.2 Parameters used in modeling nitrogen-acquiring, cellulolytic, and ligninolytic enzyme allocations..... 30

2.3 Results of ANOVA evaluating sensitivity analysis results (see section 2.3.3); proportional allocation of Type 3 partial sums of squares of ANOVA..... 46

List of Figures

1 – 1 a. Decay rate coefficients (d^{-1}) for holocellulose (solid line) and lignin (dashed line) and b. amounts (mg C g^{-1} soil) of apparent cellulolytic (solid line) and ligninolytic (dashed line) enzyme activities vs. litter LCI. 11

1 – 2 Relationships between the allocation of apparent enzyme activities (BG/[BG + OX]) and litter LCI during decomposition. Simulations with an LCI threshold = 0.4 are in solid lines and alternative model thresholds suggested by observations are shown by dashed lines: a. estimated oak litter LCI from Snajdr et al. (2011) including an alternative model LCI threshold = 0.6, b. oak litter LCI estimated from Magill and Aber (1998) including an alternative model LCI threshold = 0.45; c. maple litter LCI estimated from Magill and Aber (1998) including an alternative model LCI threshold = 0.55. Enzyme data used in b and c are from Carreiro et al. (2000)..... 13

2 – 1 Simulated (lines) and empirical (symbols) relationships between lignocellulose index (LCI) and: a. organic nitrogen (C_1; solid line and solid circles), cellulose (C_2, dashed line and open circles) and lignin (C_3; dotted line and triangles); b. observed proportional allocation of nitrogen-acquiring enzymes to total enzymes, $alpha_1 = E_1 / E_T$..... 40

2 – 2 Relationships between estimated $alpha_1$ values and lignocellulose index (LCI) of litter needed to balance microbial C:N stoichiometry (solid line), to maximize

carbon acquisition (dashed and dotted line), driven by empirically-observed enzyme activities (dotted line), and between estimated $alpha_2$ value and LCI (dashed line). 41

2 – 3 a. Relationships between overall litter decay rate (dC_i/dt) and lignocellulose index (LCI) of litter needed to balance microbial C:N stoichiometry (solid line) and driven by empirically-observed enzyme activities (dotted line); b. Relationships between simulated decay rates for pools of organic nitrogen (dC_1/dt; dotted line), cellulose (dC_2/dt; solid line), and lignin (dC_3/dt; dashed line) substrates and lignocellulose index (LCI) of litter needed to balance microbial C:N stoichiometry; and c. Relationships between simulated decay rates for pools of organic nitrogen (dC_1/dt; dotted line), cellulose (dC_2/dt; solid line), and lignin (dC_3/dt; dashed line) substrates and lignocellulose index (LCI) of litter driven by empirically-observed enzyme activities..... 43

2 – 4 Simulated relationships between calculated nitrogen (dotted line) and carbon (solid line) fluxes needed to balance microbial C:N stoichiometry at given values of lignocellulose index (LCI) of litter; the intersection of C and N fluxes estimates TER = 0.56 at a baseline CN_1 = 7.0 (middle circle), while the other circles show estimated TER = 0.55 and 0.57 with CN_1 at 6.3 and 7.7 (lowest and highest circles, respectively). 44

2 – 5 Relationships between realized carbon use efficiency of all substrates combined (CUE_T) and lignocellulose index (LCI) needed to balance microbial C:N requirements (solid line) and driven by empirically-observed enzyme activities

(dotted line), and between carbon use efficiency of the lignocellulose pool (CUE_{23}) and LCI (dashed line)..... 48

Chapter 1

Estimating Relative Cellulolytic and Ligninolytic Enzyme Activities as Functions of Lignin and Cellulose Content in Decomposing Plant Litter

Margida, M. G., Lashermes, G., & Moorhead, D. L., 2020. Estimating relative cellulolytic and ligninolytic enzyme activities as functions of lignin and cellulose content in decomposing plant litter. Soil Biology and Biochemistry, 141, 107689.

Abstract

Extracellular enzymes catalyze plant litter decomposition, including enzymes that degrade holocellulose (E_2) and lignin (E_3). To estimate relative enzyme activities associated with observed patterns of hollocellulose (C_2) and lignin (C_3) decay, we set observed decay rates equal to reverse Michaelis-Menten equations. Results were consistent with empirical studies, showing a negative relationship of $E_2/(E_2+E_3)$ to litter lignin content, $C_3/(C_2+C_3)$, above a minimum threshold at which lignin begins to decay. This threshold was previously reported to be 40% lignin content, but our results demonstrated substantial variability with litter type and environment. To our knowledge, this is the first mechanistic explanation of microbial allocation of cellulolytic and ligninolytic enzymes as a function of the lignin concentration of the lignocellulose complex but raises further questions about factors controlling the threshold for lignin decay, such as nitrogen availability.

1.1 Introduction

Various aspects of plant litter quality affect decomposition rates (Berg and Staaf 1980, Melillo et al. 1989, Bengtsson et al. 2018). An important one is the carbon quality of litter determined by the relative proportions of different chemical compounds, such as cellulose, hemicellulose and lignin. These are the main constituents of the plant cell wall and the most abundant forms of organic matter in terrestrial ecosystems (Klemm et al. 2005). However, cellulose and hemicellulose are energy rich polysaccharides whereas lignin is a polyphenolic compound and likely energy sink for catalysis (Kirk and Farrell 1987). For these reasons, the microbial carbon use efficiency (CUE; herein assumed to be the fraction of decomposed substrate carbon fixed into microbial biomass) of holocellulose is generally considered to be positive, whereas the CUE for lignin may be negative if the energetic cost of lignin decay is greater than the yield despite the possible assimilation of some lignin carbon into microbial biomass. The two compounds usually decompose at different rates and many decomposition models have long separated them into different pools (Paul and Juma 1981). In brief, microbes preferentially attack the high-energy holocellulose litter fractions during decomposition, yielding monosaccharides like glucose and xylose that are readily metabolized by microorganisms and thereby increasing the lignin concentration of remaining litter (Melillo et al. 1989). However, biochemical linkages between polysaccharides and lignin may also necessitate the breakdown of lignin to increase access to holocellulose (Sinsabaugh and Follstad Shah 2011, Talbot and Treseder 2012, Campbell et al. 2016).

Hydrolytic enzymes such as beta-glucosidases (BG) depolymerize cellulose, which has a linear chemical structure offering sequential binding sites for enzymes. In

contrast, oxidative enzymes (OX) such as phenol oxidases and peroxidases depolymerize lignin, which has an irregular structure composed of several types of linkages and subunits that limits effective binding sites for enzymes. Lignin present in plant litter affects decomposition rates by reducing holocellulose accessibility to enzymatic hydrolysis both physically (Boerjan et al. 2003) and chemically by non-specific enzyme binding (Hammel 1997). Consequently, the lignocellulose index (LCI = lignin/[lignin + hollocellulose]) of plant litter has long been a strong predictor of decomposition rate (Meentemeyer 1978, Whittinghill et al. 2012) and likely influences the microbial allocation of extracellular enzymes that catalyze the degradation of lignocellulose.

To our knowledge, the effects of LCI on the relative activities of cellulolytic and ligninolytic enzymes have not been explicitly examined. In contrast, Moorhead et al. (2013) described the control of LCI on empirical, first order decay rate coefficients (k_i) for hollocellulose (C_2 = cellulose + hemicellulose) and lignin (C_3) between LCI values ranging from 0 (plant litter contains no lignin) to 0.7 (the empirical maximum amount of lignin, defined by Melillo et al. 1982), by assuming an energetic cost-benefit relationship between C_2 and C_3 decomposition. Carbon use efficiency for C_2 was considered to be positive, whereas CUE for C_3 was negative; as LCI increased, realized CUE for lignocellulose decay decreased. Although a negative CUE seems counterintuitive, it simply represents the net cost rather than gain in energy from the degradation of lignin (Moorhead et al. 2013), a cost that is met by the net yield of energy from the degradation of holocellulose. In this model, the decay rate coefficient for holocellulose, k_2, is a piecewise, declining linear function of LCI, changing slope at an LCI value (LCI_{THR}), at which lignin begins to decay and above which the decay rate coefficient for lignin, k_3, is

an increasing linear function of LCI. Because hydrolytic enzyme activity catalyzes holocellulose decomposition, and oxidative enzyme activity drives lignin decomposition, LCI should relate to the proportion of hydrolytic and oxidative enzyme activity (Sinsabaugh 2010) needed to estimate the decay rate coefficients (k_i) for holocellulose and lignin, respectively.

To our knowledge, previous decomposition models have not included LCI as a control on enzyme expression. However, several recent models of plant litter decomposition incorporated enzyme pools using either the reverse Michaelis-Menten (RMM) or standard Michaelis-Menten (MM) equations (Tang 2015). The simplest have one substrate pool that is degraded by one enzyme (e.g., Schimel and Weintraub 2003), while the most complex include multiple enzyme pools that degrade multiple substrate pools (Allison 2005, Moorhead et al. 2012, Abramoff et al. 2017). In contrast, a suite of recent soil carbon partitioning studies (Cotrufo et al. 2015, Soong et al. 2015, Campbell et al. 2016) examined the relationship between LCI and soil organic carbon formation, but without explicitly incorporating extracellular enzyme activities. An intermediate example is the Millennial model (Abramoff et al. 2018), which used microbial biomass as a proxy for enzymes in MM formulations.

In summary, the mechanisms of plant litter decomposition are complicated by the physical and chemical links between holocellulose and lignin that require different enzymes to cleave. However, existing enzyme-based models have not addressed interactions between these substrate pools. Our goal was to develop a model to calculate the allocation of hydrolytic and oxidative enzymes to match observed decay rates of holocellulose and lignin, respectively, given litter LCI (Moorhead et al. 2013).

1.2 Modeling methods

1.2.1 Rationale

Our model balances holocellulose (C_2) hydrolysis by cellulolytic enzymes (E_2) with lignin (C_3) degradation by oxidative enzymes (E_3). A key assumption of this model is that enzyme-catalyzed reactions tend to occur at roughly half the theoretical maximum rate (k_{MAX}) (Sinsabaugh et al. 2014); thus $V_{MAX} \cong 2 \cdot k_{MAX} \cdot C$ for use in the RMM equation. The justification for this assumption is that enzymes rarely face selection pressures that would require them to operate at maximum efficiency and so moderately efficient enzymes actually optimize resource gain from multiple reactions (Bar-Even et al. 2011, Kari et al. 2019). Moreover, the half-saturation coefficients in these equations (K_M) that approximate substrate concentrations optimize the responsiveness of reaction rates (Klipp and Heinrich 1994). Thus, the relationship between V_{MAX} and K_M should be tightly constrained, as verified in a recent meta-analysis by Sinsabaugh et al. (2014). Given the above assumption, the decay of C_2 and C_3 can be estimated with the RMM equation as $dC_i/dt = (2 \cdot (k_{MAXi} \cdot C_i) \cdot E_i) / (K_{Ei} + E_i)$, where K_{Ei} is the half saturation constant for enzyme concentration (E_i) and k_{MAXi} is the maximum decay rate coefficient for first-order estimates of decomposition rates of substrates (Moorhead et al. 2013). In the present study, realized k_i varies with LCI so that the allocation of enzymes should also change with LCI. All model parameters are listed in Table 1.1:

Table 1.1: Parameters used in modelling cellulolytic and ligninolytic enzyme allocations.

Parameter	Value		Units
CUE_2	0.50	Microbial carbon use efficiency of cellulose	unitless
CUE_3	-0.21	Microbial carbon use efficiency of lignin	unitless
K_{E2}	0.30	Enzyme half saturation constant for cellulose	mg C g^{-1}
K_{E3}	0.30	Enzyme half saturation constant for lignin	mg C g^{-1}
k_{MAX2}	0.10	Maximum substrate decay rate coefficient for cellulose	d^{-1}
k_{MAX3}	0.01	Maximum substrate decay rate coefficient for lignin	d^{-1}
LCI_{MAX}	0.70	Maximum LCI	unitless
LCI_{THR}	0.40	Threshold at which lignin decay begins	unitless
m_2	-0.17	Slope of substrate decay rate coefficient for cellulose	d^{-1}
m_3	0.03	Slope of substrate decay rate coefficient for lignin	d^{-1}

The allocation of enzyme pools was determined by setting RMM functions equal to decay rates estimated by first-order equations for both holocellulose and lignin. The linear functions of k_i at given LCI described by Moorhead et al. (2013) were used in place of the decay rate coefficients in these equations. When $LCI \geq LCI_{THR}$:

$$(2 \cdot (k_{MAX2} \cdot C_2) \cdot E_2) / (K_{E2} + E_2) = (m_3 \cdot CUE_2/CUE_3 \cdot (LCI - LCI_{MAX}) + k_{MAX3}) \cdot C_2 \quad (1.1)$$

$$(2 \cdot (k_{MAX3} \cdot C_3) \cdot E_3) / (K_{E3} + E_3) = (m_3 \cdot LCI + k_{MAX3}) \cdot C_3 \quad (1.2)$$

and when $LCI < LCI_{THR}$:

$$(2 \cdot (k_{MAX2} \cdot C_2) \cdot E_2) / (K_{E2} + E_2) = (m_2 \cdot LCI + k_{MAX2}) \cdot C_2 \quad (1.3)$$

$$dC_3/dt = 0 \quad (1.4)$$

where m_i are the slopes of k_i versus LCI (Moorhead et al. 2013). These equations were then solved for E_2 and E_3 in terms of k_{MAXi}, K_{Ei}, LCI, LCI_{MAX}, and CUE_i, when $LCI \geq LCI_{THR}$:

$$E_2 = - K_{E2} \cdot (CUE_2 \cdot LCI \cdot m_3 - CUE_2 \cdot LCI_{MAX} \cdot m_3 + CUE_3 \cdot k_{MAX3}) / (CUE_2 \cdot LCI \cdot m_3 - CUE_2 \cdot LCI_{MAX} \cdot m_3 - 2 \cdot CUE_3 \cdot k_{MAX2} + CUE_3 \cdot k_{MAX3}) \quad (1.5)$$

$$E_3 = - K_{E3} \cdot (LCI \cdot m_3 + k_{MAX3}) / (LCI \cdot m_3 - k_{MAX3}) \quad (1.6)$$

and when $LCI < LCI_{THR}$:

$$E_2 = - K_{E2} \cdot (LCI \cdot m_2 + k_{MAX2}) / (LCI \cdot m_2 - k_{MAX2}) \quad (1.7)$$

$$E_3 = 0 \quad (1.8)$$

Using the parameter estimates of Schimel and Weintraub (2003) and Moorhead et al. (2013), and assuming that $K_{E2} = K_{E3}$ (Table 1.1), the only variable in equations 1.1-1.8 is LCI, assuming that CUE_2 and CUE_3 are constant. Although the values of K_E are unlikely to be identical, we found that modest variations did not substantially alter the patterns of model behavior. Thus, the relative allocations of E_2 and E_3 may be estimated by LCI of litter residue to meet empirical patterns of lignocellulose decomposition.

1.2.2 Validation

Relatively few decomposition studies report both LCI and extracellular enzyme activity (EEA) over sufficient time to show substantial changes in LCI and make it possible to define LCI_{THR} value. For example, Lashermes et al. (2016) conducted a 126-day laboratory study of lignocellulose decay in maize (*Zea mays L.)* leaves, steams, and roots inoculated with a basidiomycete (*Phanerochaete chrysosporium*). They reported a final mean LCI value of about 0.22 and a mean BG/(BG+OX) value of 0.99; thus, LCI was too low to initiate much oxidative enzyme activity. In contrast, Snajdr et al. (2011) measured mass loss, holocellulose and lignin content, and extracellular enzyme activity during oak (*Quercus petraea*) litter decomposition in a forest over two years near Prague, Czech Republic. Litter lignin content was relatively high at 38% of initial mass, and LCI values increased to approximately 0.69 by the end of the study. Although LCI was not reported on all dates of enzyme measurements, LCI was linearly related to remaining litter mass ($LCI = 0.0021 \cdot Mass + 0.5690$, $N = 5$, $R^2 = 0.8733$) and we used this relationship to estimate LCI for observed values of mass loss concurrent with all

observations of enzyme activities. We selected the activity of BG as an index to holocellulose decay and the combined activities of peroxidase and phenol oxidase (OX) as an index to lignin decay. The observed relationships between BG/(BG+OX) and LCI in decaying litter were compared to our model results.

We also constructed a second validation exercise by combining the datasets from studies by Magill and Aber (1998) and Carreiro et al. (2000). Magill and Aber (1998) conducted field decomposition studies of oak (*Quercus velutina*) and maple (*Acer rubrum*) litter over 2 years at Harvard Forest, Mass., in which they measured mass loss, lignin, and cellulose content. Although Magill and Aber (1998) did not measure EEA, final LCI values ranged 0.55-0.65. In comparison, Carreiro et al. (2000) measured mass loss and EEA during long term decomposition of oak (*Quercus rubra*) and maple (*Acer rubrum*) litter near New York, NY, but did not continuously measure lignin or cellulose content. We combined the datasets from these field studies to extrapolate relationships between EEA and LCI given mass loss patterns of similar litter types under similar field conditions. In the study by Magill and Aber (1998), LCI was linearly related to percent mass loss in decomposing oak litter ($LCI = 0.0018 \cdot Mass + 0.4554$, $N = 13$, $R^2 = 0.7503$) and maple litter ($LCI = 0.0010 \cdot Mass + 0.5368$, $N = 12$, $R^2 = 0.5226$). These relationships were used to estimate LCI at observed values of mass loss for both oak and maple litter, concurrent with observations of enzyme activities (Carreiro et al. 2000). Again, we selected the activity of BG as an index to holocellulose decay and the combined activities of peroxidase and phenol oxidase (OX) as an index to lignin decay and compared relationships between observed BG/(BG+OX) and LCI in decaying litter to our model estimates as a second validation exercise.

1.3 Results

Our model allocated holocellulose and lignin degrading enzymes in response to residue LCI as functions of carbon use efficiency similar to the pattern of first-order decay rate coefficients (Fig. 1-1). The cellulose decay rate coefficient (k_2) decreased linearly by 70% as LCI increased from 0 to 0.4 (LCI_{THR}), and by another 67% as LCI increased from 0.4 to 0.7, whereas the lignin decay rate coefficient (k_3) increased linearly from 0 to 0.01 d^{-1} as LCI increased from 0.4 to 0.7 (Fig. 1-1a). The simulated patterns of activities for cellulolytic (E_2) and ligninolytic (E_3) enzymes approximated these patterns for decay rate coefficients; the allocation of E_2 decreased by 76% as LCI increased from 0 to 0.4, and by another 74% as LCI increased from 0.4 to 0.7 (Fig. 1-1b). In contrast, E_3 increased from 0 to 0.3 mg C g^{-1} soil as LCI increased from 0.4 to 0.7 (Fig. 1-2). Despite differences in the relative magnitudes of changes in k_i's and E_i's with changing LCI, simulated enzyme activities during decay generally followed the patterns of change in empirical decay rate coefficients.

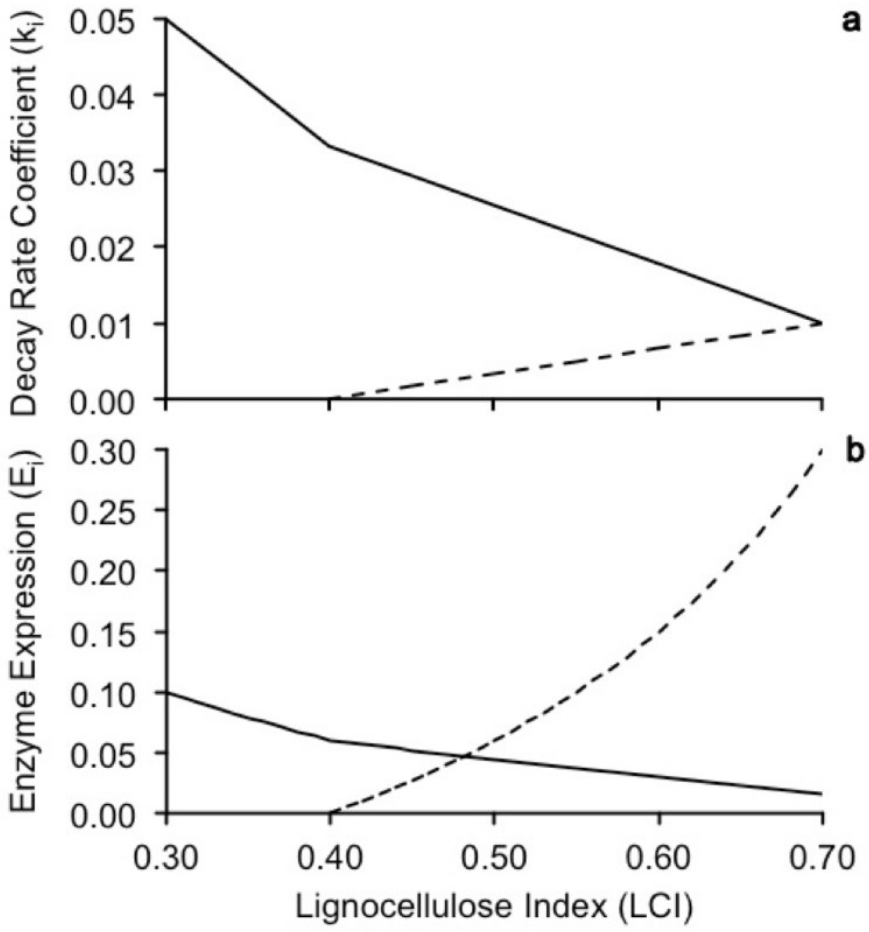

Fig. 1-1: a. Decay rate coefficients (d^{-1}) for holocellulose (solid line) and lignin (dashed line) and b. amounts (mg C g^{-1} soil) of apparent cellulolytic (solid line) and ligninolytic (dashed line) enzyme activities vs. litter LCI.

The relationships between EEA and LCI (Fig. 1-2) support the notion that tradeoffs in realized CUE balance lignin and holocellulose decay (Moorhead et al. 2013). In brief, as LCI increases during decomposition, the increased density of biochemical linkages between holocellulose and lignin necessitate the increased degradation of lignin to access holocellulose. The degradation of lignin is an energy-expensive process, defined herein as having a negative CUE (a net energy cost, as per Moorhead et al. 2013), resulting in a realized CUE for lignocellulose decomposition that declines as LCI

increases. In all cases, the relationship between BG/(BG+OX) and LCI was negative above a threshold value of LCI (LCI_{THR}), consistent with observations by Herman et al. (2008), although the LCI threshold for oxidative enzyme activity in experimental studies differed from the expected value of $LCI_{THR} = 0.4$. In the northeast USA, studies by Magill and Aber (1998) and Carreiro et al. (2000) suggested a LCI threshold for oxidative activity of about 0.45 for oak (Fig. 1-2b) and 0.55 for maple litters (Fig. 2c). In contrast, the Snajdr et al. (2011) data suggest a LCI value of about 0.60 for oak litter decomposing in the Czech Republic (Fig. 1-2a).

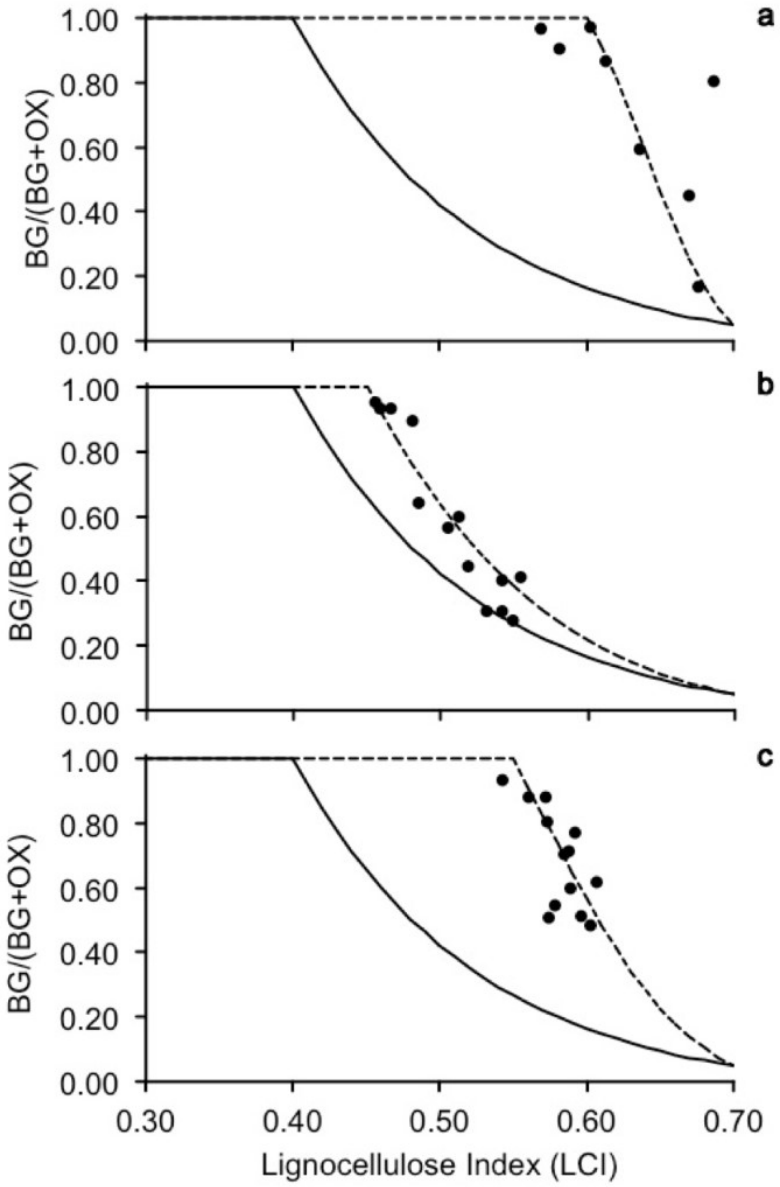

Fig. 1-2: Relationships between the allocation of apparent enzyme activities (BG/[BG + OX]) and litter LCI during decomposition. Simulations with an LCI threshold = 0.4 are in solid lines and alternative model thresholds suggested by observations are shown by dashed lines: a. estimated oak litter LCI from Snajdr et al. (2011) including an alternative model LCI threshold = 0.6, b. oak litter LCI estimated from Magill and Aber (1998) including an alternative model LCI threshold = 0.45; c. maple litter LCI estimated from Magill and Aber (1998) including an alternative model LCI threshold = 0.55. Enzyme data used in b and c are from Carreiro et al. (2000).

1.4 Discussion

Overall, model results were consistent with observed patterns of decline in proportional allocation of cellulolytic versus ligninolytic enzyme activity with increasing LCI in decaying litter despite differences between studies in the threshold value of LCI at which this proportion began to decline. To our knowledge, this represents the first attempt to calculate the allocations of enzymes associated with the degradation of the primary polysaccharide and polyphenol components of plant cell walls, which together account for the largest fraction of dead organic matter in most terrestrial ecosystems. Unfortunately, too few experimental data exist to provide additional insights to the controls on these patterns.

Variations in the apparent LCI threshold among studies may result from differences in lignin and polysaccharide assays, the oxidative enzymes measured, and characteristics of study sites. For example, Snajdr et al. (2011) measured Klason lignin and Magill and Aber (1998) used near infrared reflectance spectroscopy (NIRS) to estimate lignin content. These measuring techniques yield different values that are not necessarily comparable, e.g., Van Soest measurements are usually lower than Klason measurements (Van Soest et al. 2018). Similarly, polysaccharide assay methodology varied across these studies. Snajdr et al. (2011) measured cellulose using gas chromatography after acid hydrolysis, whereas Magill and Aber (1998) used near infrared spectroscopy (NIRS). In addition, the NIRS technique is predictive, with reflectance spectra calibrated using either Van Soest or Klason lignin and cellulose measurements, adding further variation to estimates of LCI (Brinkmann et al. 2002). For both studies, we calculated LCI based on the combined cellulose and hemicellulose content of remaining

litter, but differences measuring these polysaccharides add uncertainty to estimates of LCI.

Another source of variability when comparing studies is that differences in oxidative enzyme methods affect assay sensitivity (Bach et al. 2013). Moreover, soil microbes produce oxidative enzymes for many reasons, including ontogeny and defense as well as carbon and nitrogen acquisition (Burns et al. 2013). Thus, oxidative enzyme activity is not a direct proxy for lignin degradation. Lastly, oxidative enzyme activities are measured only in a relatively small proportion of decomposition studies (Chen et al. 2018), providing a limited suite of data for generalization. For all of these reasons, it is remarkable that our simulations showed similarities to these uncertain observations.

Finally, lignin decay is sensitive to a variety of factors. Site and litter type, as well as litter nitrogen content, have significant effects on lignin decomposition (Carreiro et al. 2000, Herman et al. 2008). Two of the decomposition studies used to validate this model (Magill and Aber 1998, Carreiro et al. 2000) took place in the northeastern USA, while the other (Snadjr et al. 2011) took place in the Czech Republic. Site differences are likely a result of variability in soil microbial communities, soil pH, atmospheric nitrogen deposition, and interactions between these controls. At global scales, the effects of nitrogen amendment on oxidative enzyme activity depend on microbial community composition and soil type (Allison et al. 2009, Burns et al. 2013). For example, Frey et al. (2014) found that nitrogen amendment of basidiomycete-dominated temperate and boreal forest soils decreased oxidative enzyme activity, while Iyyemperumal and Shi (2008) found that grassland soils dominated by glomeromycota and ascomycota showed little response. Because the LCI threshold at which oxidative enzymes become active (and

lignin decays) is responsive to multiple factors, many more data are needed to elucidate these controls than were available for this study.

In conclusion, our model predicted the proportional allocation of cellulolytic and ligninolytic enzymes during decomposition consistent with the notion that energetic tradeoffs between holocellulose and lignin decay control overall lignocellulose decomposition. This hypothesis is but one of many either proposed or previously observed to drive patterns of lignocellulose decay. Direct observation of specific enzyme activities associated with polysaccharide and polyphenol decay provides a less ambiguous explanation for these patterns than measures of changing litter chemistry and mass loss alone. Moreover, patterns of enzyme allocation with respect to LCI were consistent with a simple, underlying energy balance rationale for lignocellulose decomposition. Thus, this model integrates lignocellulose controls and extracellular enzymatic activities into a single, testable process model. However, our results also indicate that defining more precise relationships between LCI and EEA requires long-term experimental studies that couple measurements of litter chemical quality and specific enzyme assays over sufficient time to observe substantial changes in LCI.

Chapter 2

Simulating Leaf Litter Decay with Eco-enzymatic Activities Given Carbon Quality and Carbon-Nitrogen Stoichiometry

Abstract

We developed a model of plant litter decomposition including three substrate pools of organic nitrogen compounds (C_1), cellulose (C_2), and lignin (C_3), which were catalyzed by specific enzyme pools (E_1, E_2 and E_3, respectively). We then solved for the allocation of each enzyme pool as functions of litter quality, C:N stoichiometry, and constraints on total enzyme production. We first determined the proportional allocation $alpha_2 = E_2 / (E_2 + E_3)$ by setting observed decay rates at given lignocellulose index (LCI) values equal to reverse Michaelis-Menten (RMM) equations and solving for E_i. We then determined $alpha_1 = E_1 / (E_1 + E_{2+3})$, again using RMM equations, in three ways: (1) to exactly balance microbial stoichiometric needs for C and N, (2) to maximize potential C assimilation by optimizing C released from C_1 and C_{2+3} pools, and (3) using empirical observations of enzyme activity patterns. Values of $alpha_1$ and $alpha_2$ then were used to drive RMM equations estimating decomposition of all three substrates. We found that stoichiometric estimates of $alpha_1$ declined with increasing litter lignocellulose index (LCI), the C-maximizing approach increased $alpha_1$ to exclusively use C_1 at moderate

LCI, whereas the empirically observed $alpha_1$ gradually increased with LCI. Simulated patterns of litter decay and net carbon use efficiency (CUE) from these three models were similarly variable, raising questions about the stoichiometric relationships between enzyme activity, litter quality, and microbial resource demands. For example, the simulated CUE of the lignocellulose pool decreased as LCI increased although we assumed that CUE of the organic nitrogen pool remained constant. Thus, C_1 becomes an increasingly efficient source of C in recalcitrant litters, driving the rapid shift in enzyme allocation in the C-maximizing model and possibly explaining the more graduate shift in observed enzyme activities. This pattern suggests that microbes allocate an increasing amount of enzyme toward C_1 decay as decomposition progresses in order to maximize growth. Unfortunately, approximating observed patterns of $alpha_1$ with the C-maximizing model required simultaneously adjusting multiple parameters controlling relative C and N fluxes, for which we could find no set of data sufficient to inform or test this model. Finally, observed patterns of $alpha_1$ generated patterns of N-mineralization and excess C-mineralization (overflow respiration) above and below a threshold element ratio (TER) for litter C:N concentration, consistent with commonly reported patterns for litter decomposition. We conclude that this three-pool model provides a practical solution for allocating microbial C- and N-acquiring enzymes as functions of litter C-quality and C:N stoichiometry but that insufficient data exist to reconcile underlying controls with emergent patterns of C and N dynamics.

2.1 Introduction

Litter decomposition is an important biogeochemical process with global implications for nutrient cycling, C fluxes, and climate change (Neumann et al. 2018). Terrestrial ecosystems are often N-limited, so plants often meet their stoichiometric needs through N mineralized during leaf decay, making the process a key control on nutrient cycling and driver for primary production (Suseela 2019). Carbon emissions from soil organic carbon (SOC) decomposition mostly originate from the decay of the relatively labile fraction and are equal to about seven times the annual release of fossil carbon, which makes litter decomposition a significant C source to the atmosphere (Bernstein et al. 2007). However, the dynamics of litter decay and soil organic matter differ along the litter-to-soil continuum. For example, microbial carbon use efficiency (CUE) is highest in fresh, high-quality litter and lowest in highly degraded SOC (Sinsabaugh et al. 2016). Additionally, the biomass-to-substrate ratio increased from 0.1% early in decay to 15.2% in a meta-analysis that spanned multiple terrestrial systems (Su et al. 2007). Furthermore, as litter is degraded, it becomes more recalcitrant, so that the decay rate coefficient decreases along the litter-to-soil continuum.

Advances in the theory of microbial decomposition have provided a foundation for changes in the structure of fine-scale leaf decay and SOC models used in global C models. For example, Schimel and Weintraub (2003) developed a microbially-mediated enzyme-based decomposition model describing the degradation of insoluble polymers comprising the bulk of plant litter. Recently, earth system models explicitly incorporated microbial processes to increase accuracy and realism (Wieder et al. 2015), as have

global-scale SOC models (Sulman et al. 2014), smaller-scale ecosystem models (Wang et al. 2020), and those at the level of a single enzyme-substrate reaction (Tang 2015). Along with the explicit incorporation of microbial processes comes the need to balance multiple resource demands as resource qualities vary during decay.

2.1.1 Carbon-nitrogen stoichiometry

The ecological stoichiometry theory (EST) describes the balance of multiple elements needed to meet the demands of living organisms, including decomposer microorganisms (Sterner and Elser 2002) that are globally constrained at a molar C:N:P ratio in biomass at 60:7:1 (Cleveland and Liptzin 2007). Because decomposer microorganisms obtain both energy and nutrients from decaying organic matter, the threshold element ratio (TER) of soil organic matter is defined as the breakpoint between energy (C) and nutrient limitations, such as nitrogen (N) (Frost et al. 2006), e.g., $TER_{C:N} = A_N \cdot (B_{C:N} / CUE)$, where A_N is the assimilation efficiency of N, $B_{C:N}$ is the C:N ratio of biomass, and carbon use efficiency is $CUE = \mu / (\mu + R)$, in which μ is microbial growth and R is respiration. Nitrogen limitation occurs when the availability of N, relative to C, is less than TER; C limitation occurs when the reverse is true (Sinsabaugh et al. 2013). Microbial growth slows when stoichiometric needs are not met, thus slowing decomposition.

Ecoenzymatic stoichiometric theory (EEST) is based on the assumption that microbes balance their C:N requirements through the production of C- and N-acquiring enzymes (Sinsabaugh and Follstad Shah 2012). Because microorganisms degrade plant litter by depolymerizing insoluble compounds with extracellular enzymes, those enzymes

are proximal agents of plant litter decomposition (Sinsabaugh et al. 1991, 1993, 2008). For this reason, both microbial and resource stoichiometry influence extracellular enzyme activity (Sinsabaugh and Follstad Shah 2012). Most hydrolytic enzymes are substrate-specific and a relative few can be used as indicators for the acquisition of energy and nutrients from primary sources (Sinsabaugh et al. 1991, Sinsabaugh 1994). For example, beta-glucosidase (BG) is a C-acquiring enzyme that catalyzes the hydrolysis of glycosidic bonds to release glucose whereas N-acetyl glucosaminidase (NAG) and leucine aminopeptidase (LAP) are N-acquiring enzymes, attacking chitin and protein, respectively. LAP catalyzes the hydrolysis of amino acids from the N-terminus of polypeptide chains, while NAG catalyzes the hydrolysis of terminal non-reducing amide residues from oligosaccharides. The relative activities of BG, NAG and LAP can be used to indicate the relative catalysis of cellulose, chitin, and protein, respectively. Because enzymes are energetically and nutritionally expensive to produce, microbes control the relative expression of different enzymes to optimally meet energy and nutrient needs (Sinsabaugh et al. 2008, Sinsabaugh and Follstad Shah 2012). For example, the balance of relative C- and N-acquiring extracellular enzyme activities $EEA_{C:N} \approx B_{C:N} / L_{C:N} \approx TER_{C:N} / B_{C:N} = A_N / CUE$, where $EEA_{C:N} = BG / (LAP + NAG)$, and $L_{C:N}$ is the C:N ratio of labile organic material.

Although many decomposition models variously incorporate stoichiometry and nutrient dynamics (see review by Manzoni and Porporato 2009), fewer incorporate enzyme activities linking substrate and biomass stoichiometry during decay (e.g., Allison 2010, Wang and Allison 2019, Fatichi et al. 2019). In general, as litter decomposes, its C:N ratio decreases because microbes release C through respiration, while N persists due to

immobilization and possibly condensation reactions (Melillo et al. 1982, Preston et al. 2009). As resources become N-limited, CUE also decreases (Vicca et al. 2012), altering resource demands (Sinsabaugh et al. 2013). Thus, stoichiometric constraints are interactively and dynamically changing during decomposition and likely influencing enzyme expression.

2.1.2 Carbon quality

The bulk C:N ratio of litter provides little information about relative C and N accessibility ($L_{C:N}$; above) without also considering carbon quality. For example, the rate of degradation of lignocellulose depends on lignin content or lignocellulose index of the litter, i.e., LCI = C_3 / (C_3 + C_2), which affects CUE (Meentemeyer 1978, Whittinghill et al. 2012, Moorhead et al. 2013), and N accessibility when bound in polyphenolic polymers that are difficult to degrade (Rillig et al. 2007). Because both LCI and CUE are related to C and N accessibility, all four factors: LCI, CUE, and both C and N availability are related, and together influence microbial C and N acquisition. For example, the LCI model developed by Moorhead et al. (2013) estimates the relative decay rates of hollocellulose and lignin with LCI, suggesting that the relative allocation of enzymes that catalyze their breakdown follows a similar pattern. The recent model by Margida et al. (2020; Chapter 1), confirmed these relationships between litter quality (LCI) and patterns of cellulolytic (E_2) and ligninolytic (E_3) enzymes. However, neither of these models considered the effects of substrate LCI on the stoichiometric controls to decomposition.

Carbon quality (e.g., LCI) thus is likely an important control on enzyme allocation to meet stoichiometric demands (Sinsabaugh 2010, Sinsabaugh and Follstad Shah 2011,

2012). The threshold element ratio ($TER_{C:N}$) depends on microbial carbon use efficiency (CUE), which is also a function of LCI. Additionally, the C:N ratio of labile organic material ($L_{C:N}$) likely reflects the recalcitrance of substrate (i.e., LCI). Moreover, the relative availability of substrate C and N ($S_{C:N} = [1 / EEA_{C:N}] \cdot [B_{C:N} / L_{C:N}]$) depends on a half-saturation constant ($K_{C:N}$) reflecting the stoichiometry of C:N availability (Sinsabaugh and Follstad Shah 2012). Thus, the relative recalcitrance of substrate alters emergent stoichiometric relationships (Sinsabaugh 2010, Sinsabaugh and Follstad Shah 2011). To our knowledge, these relationships have not been explicitly incorporated into an enzyme-based decomposition model. This is a potentially valuable integration of controls because the relationships between LCI, $TER_{C:N}$, CUE, $L_{C:N}$, $S_{C:N}$, and $K_{C:N}$ make it clear that the concept of nutrient limitation must include an interactive measure of substrate recalcitrance.

2.1.3 Empirical evidence

Few data are available to inform such an enzyme-based decomposition model because few experimental studies have simultaneously examined the dynamics of changing litter recalcitrance and nutrient stoichiometry as well as the stoichiometry of extracellular enzymes during long-term litter decay. However, combined studies of oak and maple litter (Carreiro et al. 2000) and oak litter (Snajdr et al. 2011) decomposition revealed that lignocellulose-degrading enzymes (E_{2+3}) accounted for ~60% of total enzyme activity as LCI approached 0.7, considered to be the endpoint of LCI during decay (Melillo et al. 1982, Herman et al. 2008). The N-acquiring enzyme activities (E_1) accounted for the other 40%. In addition, long-term studies of changes in chemistry of similar litter types provided

estimates of lignin, cellulose and organic N fractions during decomposition (Aber et al. 1984, Magill and Aber 1998). Together, these studies provide a synthetic set of data combining measures of litter recalcitrance, nutrient stoichiometry, and extracellular enzyme activities during long-term litter decay.

This composite data set also raises questions. For example, the proportional contribution of N-acquiring enzymes to total enzymes ($alpha_1 = E_1 / [E_1 + E_2 + E_3]$) increased as LCI increased, although earlier work suggested an inverse relationship as realized CUE declined with increasing LCI (Moorhead et al. 2012). Also, observed ratios of C- and N-acquiring enzyme activities suggest that CUE of lignocellulose is positive at LCI = 0.7, despite earlier assumptions that it approached zero (Moorhead et al. 2013), or that microbes are mining N from recalcitrant organic matter given an external C source (e.g., priming effect; Kuzyakov 2010), or that microbes are mining C from organic N substrates (Mori 2020) to maximize microbial C-acquisition (Averill 2014). Regardless, these patterns indicated that enzyme activities are controlled differently than previously thought.

2.1.4 Objectives

Our goals are to develop a mechanistic model of enzyme-mediated litter decomposition integrating ecological stoichiometric theory and litter recalcitrance, challenge that model against empirically observed data and thereby evaluate these interacting controls on microbial allocation of C- and N-acquiring enzymes during extended litter decay. Our modeling approach is to calculate the allocations of N-acquiring, cellulolytic, and ligninolytic enzyme activities in response to changing litter LCI and C:N

contents during decomposition using reverse Michaelis-Menten equations (Schimel and Weintraub 2003) that balance the decomposition rates of these substrates with microbial demands. We then test this model with litter chemistry and enzyme data derived from combining detailed studies of long-term changes in leaf litter chemistry during decomposition with parallel patterns of enzyme activities. Our working hypothesis is that the relative C yield (CUE_{2+3}) for the lignocellulose complex will decline as LCI increases during progressive decomposition, driving a decline in the relative allocation of cellulolytic enzymes ($alpha_2 = E_2 / [E_2 + E_3]$). A decline in $alpha_2$ reduces the relative demand for N to meet microbial stoichiometric needs, thus reducing relative enzyme allocation to N-acquisition ($alpha_1$). Alternatively, $alpha_1$ may increase as the relative C yield of lignocellulose falls below the C yield of N containing compounds (CUE_1) as microorganism seek to maximize growth.

2.2 Modeling methods

Our modeling rationale is based on two earlier models of plant litter decomposition that utilized reverse Michaelis-Menten (RMM) formulations to simulate the controls of either litter recalcitrance (Margida et al. 2020) or stoichiometry (Moorhead et al. 2012), separately. First, Margida et al. (2020) balances cellulolytic and ligninolytic enzyme activities as functions of LCI by setting observed, first-order decay rates equivalent to reverse Michaelis-Menten (RMM) functions and solving for the allocation of cellulolytic and ligninolytic enzymes necessary to meet empirical decay rates. This provides both the allocation of cellulolytic enzymes necessary for lignocellulose decay ($alpha_2$) and the relative yield of C from the lignocellulose pool (CUE_{2+3}). Second, Moorhead et al. (2012)

similarly determines the allocation of C- and N-acquiring enzyme activities needed to balance microbial stoichiometric requirements given the C:N content of an organic N substrate and C quality of a C-only substrate. Herein we combine these models, using the lignocellulose model to calculate the effects of LCI on the quality of the C-only substrate and the stoichiometric model to balance C-acquisition from lignocellulose with C and N from the organic N substrate. The lignocellulose model also calculates the allocation of lignocellulolytic enzymes ($alpha_2$) whereas the stoichiometric model calculates the allocation of N- and C-acquiring enzymes ($alpha_1$).

2.2.1 Empirical data and observations

We informed our model with empirical data from several experimental studies. First, we estimated patterns of substrate pool sizes C_2 and C_3 as linear functions of LCI based on extensive field studies by Aber et al. (1984), which did not include enzyme activities but serves as one of the most detailed examinations of changes in plant litter chemistry during long term decomposition. In this study, LCI was linearly related to mass loss at later stages of decay (e.g., when LCI > 0.4) in maple, aspen, and oak leaf decomposition on Blackhawk Island, Wisconsin, USA. Next, we estimated an organic N substrate pool (C_1) by multiplying the total litter N by an assumed constant for the C:N ratio of the C_1 pool ($CN_1 = 7$), which was also linearly related to reported LCI (Table 2.1). We then defined C_T as the sum of the three litter pools ($C_T = C_1 + C_2 + C_3$), subtracted C_1 to estimate the lignocellulose pool ($C_{2+3} = C_T - C_1$), calculated lignin as a fraction of lignocellulose ($C_3 = LCI \cdot C_{2+3}$), and cellulose as the difference between lignocellulose and lignin ($C_2 = C_{2+3} - C_3$) (Table 2.1). We also estimated the size of a labile fraction of the

litter (L) that did not contain N and we assumed was not degraded by extracellular enzymes but influences decomposition processes and microbial carbon use efficiency (below). This pool was estimated as the difference between total reported litter mass and the sum of C_1 + C_2 + C_3 pools.

Table 2.1: Linear equations used to estimate model drivers.

	Equation	N	R^2	Source
C_1	20.077 · LCI + 3.015	72	0.6507	Aber et al. 1984; Magill & Aber 1998
L	-72.193 · LCI + 52.314	48	0.6383	Aber et al. 1984
LCI	0.002 · Mass + 0.455	13	0.7503	Magill & Aber 1998 (oak litter)
LCI	0.001 · Mass + 0.537	12	0.5226	Magill & Aber 1998 (maple litter)
LCI	0.002 · Mass + 0.569	5	0.8733	Snajdr et al. 2011 (oak litter)
$alpha_1$	1.700 · LCI - 0.793	35	0.7691	Magill & Aber 1998, Carreiro et al. 2000, Snajdr et al. 2011

We then combined a dataset reporting LCI (Magill and Aber 1998) with one that reported EEA (Carreiro et al. 2000) to couple LCI and EEA measurements for the decomposition of oak and maple litters under similar environmental conditions in similar forest types, for consistency with a previous modeling study (Margida et al. 2020). LCI was linearly related to mass loss in both decomposing oak and maple litter (Table 1.1) in

the study by Magill and Aber (1998) and used to estimate LCI at observed values of mass loss for both litter types in studies by Carreiro et al. (2000), concurrent with observed enzyme activities. In the study by Snajdr et al. (2011), LCI was not reported on all dates of enzyme measurements but also was linearly related to remaining litter mass in decomposing oak litter and this relationship was used to estimate LCI for observed values of mass loss concurrent with observations of enzyme activities (Table 2.1). We then estimated the proportional allocation of N-acquiring enzymes ($alpha_1 = E_1 / [E_1 + E_2 + E_3]$) as a linear function of LCI for the combined data (Magill and Aber 1998, Carreiro et al. 2000, Snajdr et al. 2011).

The resulting estimates of relative litter pool sizes and associated enzyme activities were used to interpret C and N fluxes during decomposition. Data from the Aber et al. (1984) study were used to define general relationships between LCI and C_1, C_2, C_3 and L over long-term decomposition (above). Combined, the Magill and Aber (1998), Carreiro et al. (2000), and Snajdr et al. (2011) studies provided enzyme data coupled with LCI values during the decomposition of similar species in comparable deciduous forests. Overall, the combined data sets aligned EEA, LCI, C_i and N (in C_1) used to address the objectives of this study.

2.2.2 Modeling rationale

Balancing microbial C:N stoichiometric requirements for growth (Eq. 2.1, below) by balancing the activities of the enzyme pools depends on three factors. First, LCI controls the expected decay rates of C_2 and C_3 and thus C_{2+3} (Herman et al. 2008, Moorhead et al. 2013). Second, the C yield from C_1 and from the lignocellulose complex (C_{2+3}) to support

microbial growth should balance the N yield from C_1 (Eq. 2.1). Third, total enzyme production ($E_T = E_1 + E_2 + E_3$) constrains the amount of enzyme allocated to degrade C_1 and C_{2+3}. Our model assumes the decomposition of the organic N pool (C_1) by N-acquiring enzymes (E_1), cellulose (C_2) hydrolysis by cellulolytic enzymes (E_2), and lignin (C_3) degradation by oxidative enzymes (E_3). This model allocates enzymes among the three pools according to three main drivers: substrate lignin concentration (LCI), litter N content (CN_1), and the total microbial enzyme pool (E_T). Variations in total microbial enzyme pool size alter both relative decay rates and enzyme allocation because rates of decay are nonlinear functions of enzyme concentrations (below). We herein present a practical approach to determine the allocation of E_1, E_2, and E_3 as hierarchically nested functions of LCI, CN_1, and E_T. All model parameters are listed in Table 2.2.

Table 2.2: Parameters used in modeling nitrogen-acquiring, cellulolytic, and ligninolytic enzyme allocations.

Parameter	Value		Units
B:S	0.02	Biomass-to-substrate ratio (carbon)	unitless
CN_1	7.00	C:N ratio of organic N	mg C/mg N
CN_M	7.16	C:N ratio of microbial biomass	mg C/mg N
CUE_1	0.40	Microbial carbon use efficiency of organic N	unitless
CUE_2	0.60	Microbial carbon use efficiency of cellulose	unitless
CUE_3	-0.3	Microbial carbon use efficiency of lignin	unitless
E:B	0.02	Enzyme-to-biomass ratio (carbon)	unitless
K_{E1}	0.30	Enzyme half saturation constant for organic N	mg C/g
K_{E2}	0.30	Enzyme half saturation constant for cellulose	mg C/g
K_{E3}	0.30	Enzyme half saturation constant for lignin	mg C/g
k_{MAX1}	0.20	Maximum substrate decay rate coefficient for organic N	d^{-1}
k_{MAX2}	0.10	Maximum substrate decay rate coefficient for cellulose	d^{-1}
k_{MAX3}	0.01	Maximum substrate decay rate coefficient for lignin	d^{-1}
LCI_{MAX}	0.70	Maximum lignocellulose index	unitless
LCI_{MID}	0.40	Threshold at which lignin decay begins	unitless
m_2	-0.2	Slope of substrate decay rate coefficient for cellulose	d^{-1}
m_3	0.03	Slope of substrate decay rate coefficient for lignin	d^{-1}

2.2.3 Carbon- and nitrogen- acquiring enzyme allocation

We first assume that microbes produce C- and N-acquiring enzymes to decompose two different types of organic matter pools, one that contains nitrogen (C_1) and a lignocellulose pool that contains only carbon (C_{2+3}), to meet their stoichiometric requirements (Sinsabaugh and Follstad Shah 2012). Note that cellulose and lignin are combined into a single composite pool at this step:

$$CN_B = CN_1 \cdot (CUE_1 \cdot dC_1/dt + CUE_{2+3} \cdot dC_{2+3}/dt) / (dC_1/dt) \quad (2.1)$$

where CN_B = microbial C:N ratio, dC_i/dt = decomposition rate for substrate (i), CN_1 = C:N ratio for pool C_1, CUE_i = carbon use efficiency for substrate (i), and assuming potential N use efficiency is 100%. Both first-order decay rates and Reverse Michaelis-Menten (RMM) equations are used to describe substrate decomposition rates (dC_i/dt):

$$k_i \cdot C_i = 2 \cdot k_{MAXi} \cdot C_i \cdot E_i / (K_{Ei} + E_i) \quad (2.2)$$

where the maximum velocity of the reaction (V_{MAXi}) is equivalent to the product, $2 \cdot k_{MAXi} \cdot C_i$ (Margida et al. 2020), k_i is the empirically observed rate coefficient, the maximum potential decay rate coefficient is k_{MAXi}, and K_{Ei} is the half-saturation coefficient of enzymes E_i on substrate C_i (Moorhead and Weintraub 2018). Hence, k_i is an empirically derived coefficient based on observations that LCI determines the rate of lignocellulose decay (Moorhead et al. 2013). Equation 2.2 was reordered to estimate the amount of enzyme needed to meet the expected decay rate:

$$E_i = -k_i \cdot K_{Ei} / (k_i - 2 \cdot k_{MAXi}) \quad (2.3)$$

The resulting estimates of E_1 and E_{2+3} were summed to estimate the total enzyme pool (E_T), and $alpha_1 = E_1 / E_T$ was defined as the proportional allocation of N-acquiring to total enzymes (see appendix A for equation).

An alternative rationale to exactly matching the stoichiometric demands of microorganisms for C and N was to maximize microbial growth (μ), i.e., C assimilation by altering equation 2.1:

$$\mu = CUE_1 \cdot dC_1/dt + CUE_{2+3} \cdot dC_{2+3}/dt \quad (2.4)$$

The decay rates in equation 2.4 were replaced with their respective RMM equations (Eq. 2.2) and respective enzyme pool sizes defined as $E_1 = alpha_1 \cdot E_T$ and $E_2 = (1 - alpha_1) \cdot E_T$. Conditions generating maximum μ were determined by setting the derivative $d\mu/d(alpha_1)$ to zero and solving for $alpha_1$ (appendix A). Thus, we calculated two estimates of $alpha_1$ based on anticipated enzyme activities, one that exactly balanced the stoichiometric demands of microorganisms (Eq. 2.1) and another that maximized microbial growth (Eq. 2.4).

2.2.4 LCI controls

The first-order decay rate coefficients for cellulose (k_2) and for lignin (k_3) (eqs. 2, 3) are described as linear functions of LCI (Moorhead et al. 2013), and thus the ratio of k_3:k_2 is constant at any LCI regardless of the actual rate of lignocellulose decomposition. Equation 2.3 was used to calculate E_2 and E_3 for the expected values of k_2 and k_3, given pool sizes C_2 and C_3 (Eq. 2.2). We then assumed that the relationship between the decomposition rate of the combined lignocellulose ($C_{2+3} = C_2 + C_3$) pool and total

lignocellulolytic enzyme pool ($E_{2+3} = E_2 + E_3$) at any LCI could be approximated as a composite RMM_{2+3} equation:

$$dC_{2+3}/dt = V_{MAX2+3} \cdot E_{2+3} / (K_{E2+3} + E_{2+3}) \quad (2.5)$$

where the maximum velocity of the reaction (V_{MAX2+3}) is equivalent to the product, $2 \cdot k_{MAX2} \cdot C_2 + 2 \cdot k_{MAX3} \cdot C_3$ (Margida et al. 2020). The left side of equation 2.5 was estimated as the sum of first-order decay rates for C_2 and C_3 (left side of Eq. 2.2), such that $dC_{2+3}/dt = k_2 \cdot C_2 + k_3 \cdot C_3$, given LCI. The first-order rates for dC_2/dt and dC_3/dt were individually set equivalent to their respective RMM_i equations to estimate enzyme concentrations (E_i) needed to meet these rates (Eq. 2.3). The resulting estimates of E_2 and E_3 were summed to estimate the total lignocellulolytic enzyme pool (E_{2+3}), and $alpha_2$ was defined as the proportional allocation of cellulolytic to total lignocelluloytic enzymes ($E_{2+3} = E_2 / (E_2 + E_3)$). The value of K_{E2+3} was then estimated by reorganizing equation 2.5.

If decay rates are less than maximum, the ratio of ligninolytic (E_3) to cellulolytic enzymes (E_2) can vary at a given LCI because the RMM equations are saturating functions of E and likely have different kinetic coefficients for lignin and cellulose (Eq. 2.2). For this reason, restrictions on enzyme pool size (E_T) must be included in balancing E_i's.

2.2.5 E_T controls

The effects of variations in total enzyme pool size (E_T) on the allocation of cellulolytic and ligninolytic enzymes were evaluated by calculating alternative potential decay rates for C_{2+3} and their associated enzyme concentrations at a given LCI (section 2.2.2) and then deriving V_{MAX2+3} and K_{E2+3} following the Lineweaver-Burk method. For example, the maximum expected rate of decomposition was based on the expected values

of the decay rate coefficients (Eq. 2.2) at a given LCI and pool sizes for C_2 and C_3, and then used to calculate associated values of E_2 and E_3 (Eq. 2.5). An alternative rate was calculated by reducing these decay rate coefficients to a fraction (s) of their expected values, i.e., $k_{2S} = s \cdot k_2$. The resulting estimates of maximum and reduced reaction rates and enzyme concentrations (Eq. 2.5) were inverted and the linear relationship between the inverses of decay rates and the inverses of enzyme concentrations produced slope = K_{E2+3} / V_{MAX2+3} and intercept = $1 / V_{MAX2+3}$ values (Lineweaver and Burk 1934). In this manner, the kinetic coefficients of equation 2.5 were approximated at any given LCI, and the impacts of enzyme pool size (E_T) on decomposition and enzyme allocation were quantified.

2.2.6 Balancing C and N fluxes

Empirical observations of relative substrate pool sizes and enzyme activity patterns (section 2.1.1) were used to drive RMM equations estimating decomposition. We assumed that E_T was approximately $0.004 \cdot C_T$, i.e., that microbial biomass was approximately 2% of total system C and that enzyme allocation was approximately 2% of microbial biomass (Schimel and Weintraub 2003, Sinsabaugh et al. 2016). We also assumed that the half-saturation coefficients for carbon pools scaled with their relative concentrations, i.e., $K_{E(i)}$ = Maximum $K_{E(i)} \cdot [C_i / (C_T)]^{1/3}$, using the cube-root to roughly account for enzyme diffusion through three dimensions. We then calculated carbon flux (R_O) needed to balance C and N flows from litter to microbes given values of C_1, C_2, C_3 and $alpha_1$ by adding a C-flux term (R_O) to the basic C and N balance equation (appendix A) when $alpha_1$ is given. This was calculated by modifying equation 2.1 to include R_O:

$$CN_B = (CUE_1 \cdot dC_1/dt + CUE_{2+3} \cdot dC_{2+3}/dt + R_O) / ((dC_1/dt) / CN_1) \quad (2.6)$$

A positive value of R_O indicates a surplus of C released by enzyme activities with respect to N, needed to balance microbial C:N demands (Eq. 2.1). This surplus is sometimes termed "overflow respiration" (Schimel and Weintraub 2003). A negative value indicates a C deficit with respect to N released from decomposition.

Similarly, we calculated nitrogen flux (N_M) needed to balance C flows from litter decomposition estimated according to enzyme activities and substrate quality by adding N_M to the basic C and N balance equation (appendix A) when $alpha_1$ is given. This was calculated by modifying equation 2.1 to include N_M:

$$CN_B = (CUE_1 \cdot dC_1/dt + CUE_{2+3} \cdot dC_{2+3}/dt) / ((dC_1/dt) / CN_1 + N_M) \quad (2.7)$$

A positive value of N_M indicates a deficit of N released by enzyme activities with respect to C, needed to balance microbial C:N demands (Eq. 2.1). This is an estimate of potential N immobilization. A negative value indicates a N surplus with respect to C released from decomposition, or potential N mineralization.

The point at which a C surplus switches to a deficit is commonly known as the threshold element ratio (TER) and corresponds to the point at which a N deficit switches to a surplus (Frost et al. 2006). Although this value is traditionally expressed as the microbial biomass C:N ratio divided by carbon use efficiency (above), this approach assumes constant substrate and microbial biomass stoichiometry and constant product assimilation efficiencies (both N and C) throughout decomposition. Neither assumption is true. Substrate stoichiometry clearly changes during decay and CUE varies both with substrate stoichiometry (Moorhead et al. 2012) and LCI (Moorhead et al. 2013). Herein we approximated TER as the intersection of R_O and N_M, which occurs only when both values are zero.

We estimated cumulative C loss from litter decay and both positive and negative values of R_O, based on decay rates at given values of LCI and the relationship between litter mass and LCI (section 2.1.1) to translate decay rates into C loss. We followed the same procedure with simulated N immobilization and mineralization (N_M). We also calculated the total amount of C potentially fixed into biomass at each LCI:

$$C_F = (CUE_1 \cdot dC_1/dt + CUE_{2+3} \cdot dC_{2+3}/dt) \quad (2.8)$$

We then integrated all estimates of C_F across all values of LCI (and mass loss) to generate an overall estimate of microbial C uptake for the entire range of decomposition.

2.2.7 Carbon use efficiency

We estimated a composite CUE in two ways. First, we calculated it within the model as a function of dC_1/dt and dC_{2+3}/dt:

$$CUE_T = (CUE_1 \cdot dC_1/dt + CUE_{2+3} \cdot dC_{2+3}/dt) / (dC_1/dt + dC_{2+3}) \quad (2.9)$$

We also estimated CUE stoichiometrically as a function of labile resource availability (Sinsabaugh et al. 2016):

$$CUE_{C:N} = CUE_{MAX} \cdot (S_{C:N} / (S_{C:N} + K_{C:N})) \quad (2.10)$$

where CUE_{MAX} is the empirical maximum carbon use efficiency (Sinsabaugh and Follstad Shah 2012), $S_{C:N}$ is the relative availability of substrate C and N ($S_{C:N} = [1 / EEA_{C:N}] \cdot [B_{C:N} / L_{C:N}]$), and $K_{C:N}$ is a half-saturation constant (0.5) reflecting the stoichiometry of C:N availability (Sinsabaugh and Follstad Shah 2012). This $CUE_{C:N}$ estimate relied upon the C:N ratio of the entire labile fraction of the litter ($L_{C:N}$) as a function of L, C_1, and CN_1:

$$L_{C:N} = (L + C_1) / (C_1 / CN_1) \quad (2.11)$$

We then compared CUE_T and $CUE_{C:N}$ between models.

2.2.8 Sensitivity analysis

We conducted a sensitivity analysis to gauge model behavior given the observed enzyme activity patterns in response to variation in key parameters: the C:N ratio of organic nitrogen (CN_1), the microbial carbon use efficiency of the cellulose pool (CUE_2), the LCI threshold for lignin decay (LCI_{MID}), and the exponent for the half-saturation coefficient for enzymes operating on substrate (EXP). We chose these parameters because they are indicators of C:N stoichiometry (CN_1), carbon quality (CUE_2 and LCI_{MID}), and enzyme activity (EXP), respectively. We examined model outputs driven by the observed values of $alpha_1$, including threshold element ratio (TER), cumulative overflow respiration (R_O), cumulative nitrogen mineralization (N_M), and total amount of litter decay (dC_T/dt) over the observed range of litter LCI.

We simultaneously varied all four selected model parameters 1000 times with uniform random distributions within a 20% range of baseline values. We varied CN_1 between 6.3 and 7.7 (Sterner and Elser 2002, Miller 2000, Trofymow et al. 1983), CUE_2 between 0.48 and 0.60 (given a theoretical 0.6 maximum; Sinsabaugh et al. 2014), LCI_{MID} between 0.36 and 0.44 ($0.4 \pm 20\%$; Hermann et al. 2008), and EXP between 0.30 and 0.37. Of the 1000 random values generated for each parameter, a total of 1000 random sets of the four parameter estimates were selected (Latin hypercube method) for statistical analysis. A general linear model compared variations in output variables (TER, $\sum R_O$, $\sum N_M$, and $\sum dC_T/dt$) to variations in the parameters (CN_1, CUE_2, LCI_{MID}, and EXP). The type 3 partial sums of squares attributed to each parameter were compared to the total contributions of variations in all parameters to variations in model output variables to estimate the proportional contributions of each parameter to each output variable.

2.3 Results

2.3.1 Litter and enzyme pools

Overall, both the relative amounts of organic nitrogen (C_1) and lignin (C_3) substrate pools in decomposing litter increased with LCI and the relative cellulose (C_2) content decreased, as would be expected during progressive decay (Fig. 2-1a). As LCI increased from 0.47 to 0.67, C_1 increased by 46.6%, from 11.6 to 17.0% of remaining litter mass, C_2 decreased by 41.5%, from 46.8 to 27.4%, and C_3 increased by 34%, from 41.5 to 55.6%. The proportional allocation of N-acquiring enzymes ($alpha_1$) also increased with LCI (Fig. 2-1b, Fig. 2-2), from the lowest observed value of 0.03 at LCI = 0.47 to 0.30 at LCI = 0.67. This observed pattern of $alpha_1$ also was used to drive the estimated rates of decay, given relative enzyme pool sizes and relative substrate pool sizes, assuming a total enzyme pool size (E_T) representing the fraction 0.004 of the total litter carbon (Eq. 2.3, Sec. 2.2.3).

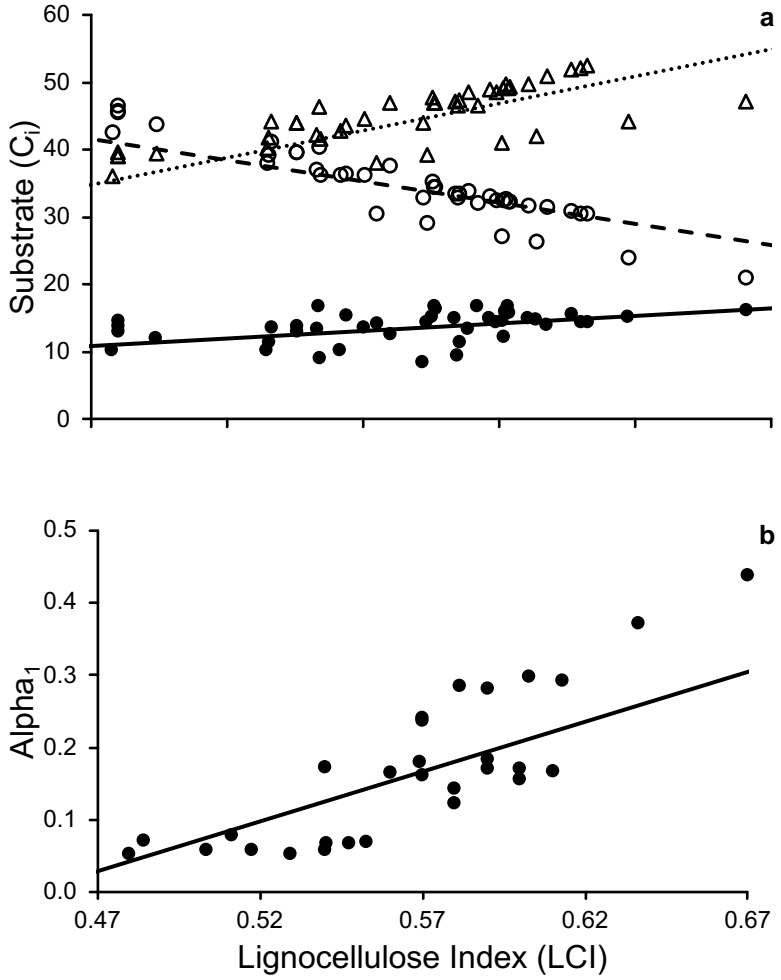

Fig. 2-1: Simulated (lines) and empirical (symbols) relationships between lignocellulose index (LCI) and: a. organic nitrogen (C_1; solid line and solid circles), cellulose (C_2, dashed line and open circles) and lignin (C_3; dotted line and triangles); b. observed proportional allocation of nitrogen-acquiring enzymes to total enzymes, $alpha_1 = E_1 / E_T$.

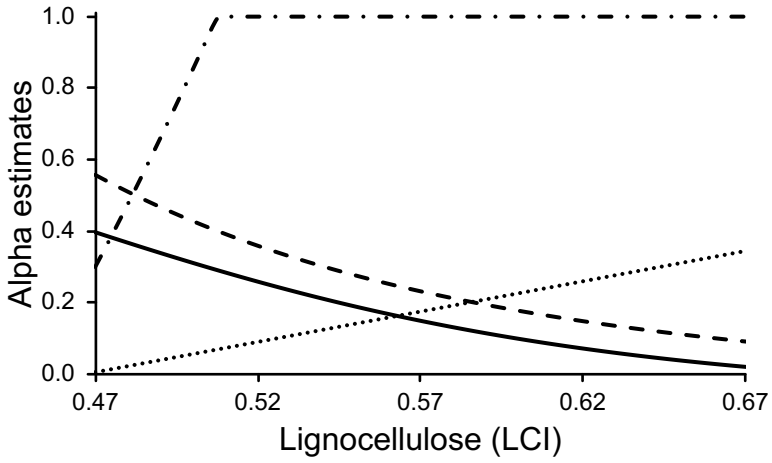

Fig. 2-2: Relationships between estimated alpha$_1$ values and lignocellulose index (LCI) of litter needed to balance microbial C:N stoichiometry (solid line), to maximize carbon acquisition (dashed and dotted line), driven by empirically-observed enzyme activities (dotted line), and between estimated alpha$_2$ value and LCI (dashed line).

2.3.2 General model behavior

When alpha$_1$ was estimated to exactly balance microbial C:N requirements (the stoichiometric model), the calculated decay rates of organic nitrogen (dC_1/dt) and cellulose (dC_2/dt) substrate pools based on RMM equations (Eq. 2.2) decreased with LCI, while lignin decay (dC_3/dt) increased (Fig. 2-3b). For example, as LCI increased from 0.47 to 0.67, dC_1/dt decreased from 0.475 to 0.034, dC_2/dt decreased from 0.509 to 0.095, and dC_3/dt increased from 0.038 to 0.141 (all decay rates are expressed in units C per day given 100 units of total substrate C, i.e., as percent of the total litter remaining). Total, cumulative substrate decay (dC_T/dt = dC1/dt + dC2/dt + dC3/dt) between LCI 0.47 and 0.67 was 36% of the initial substrate C.

Alternatively, when alpha$_1$ was estimated to maximize microbial growth (μ), the calculated decay rate of the organic N (dC_1/dt) substrate pool based on RMM equations

(Eq. 2.2) increased with LCI, while cellulose (dC_2/dt) decreased and lignin (dC_3/dt) decay varied. For example, as LCI increased from 0.47 to 0.67, dC_1/dt increased from 0.37 to 1.29, dC_2/dt decreased from 0.59 to 0.00, and dC_3/dt decreased from 0.04 to 0.00. We could approximate the observed pattern of $alpha_1$ in the maximum growth model only by simultaneously varying multiple parameters, including CN_1, CUE_i, K_{Ei}, k_{max1}, B:C, and E:B (not shown), beyond any of the observed data or theoretical relationships cited herein. For this reason, we focused the rest of our study on the stoichiometric and empirical models.

In contrast to the stoichiometric model, when observed values of $alpha_1$ drove simulations (the empirical model), the calculated decay rates of organic nitrogen (dC_1/dt) and lignin (dC_3/dt) substrate pools based on RMM equations (Eq. 2.2) increased with LCI, while cellulose decay (dC_2/dt) decreased (Fig. 2-3c). For example, as LCI increased from 0.47 to 0.67, dC_1/dt increased from 0.008 to 0.511, dC_2/dt decreased from 0.809 to 0.066, and dC_3/dt increased from 0.060 to 0.098 (as above, all decay rates are expressed in units C per day given 100 units of total substrate C, i.e., as percent of the total litter remaining). Total, cumulative substrate decay ($dC_1/dt+dC_2/dt+dC_3/dt$) between LCI 0.47 and 0.67 was 46% of the initial substrate C.

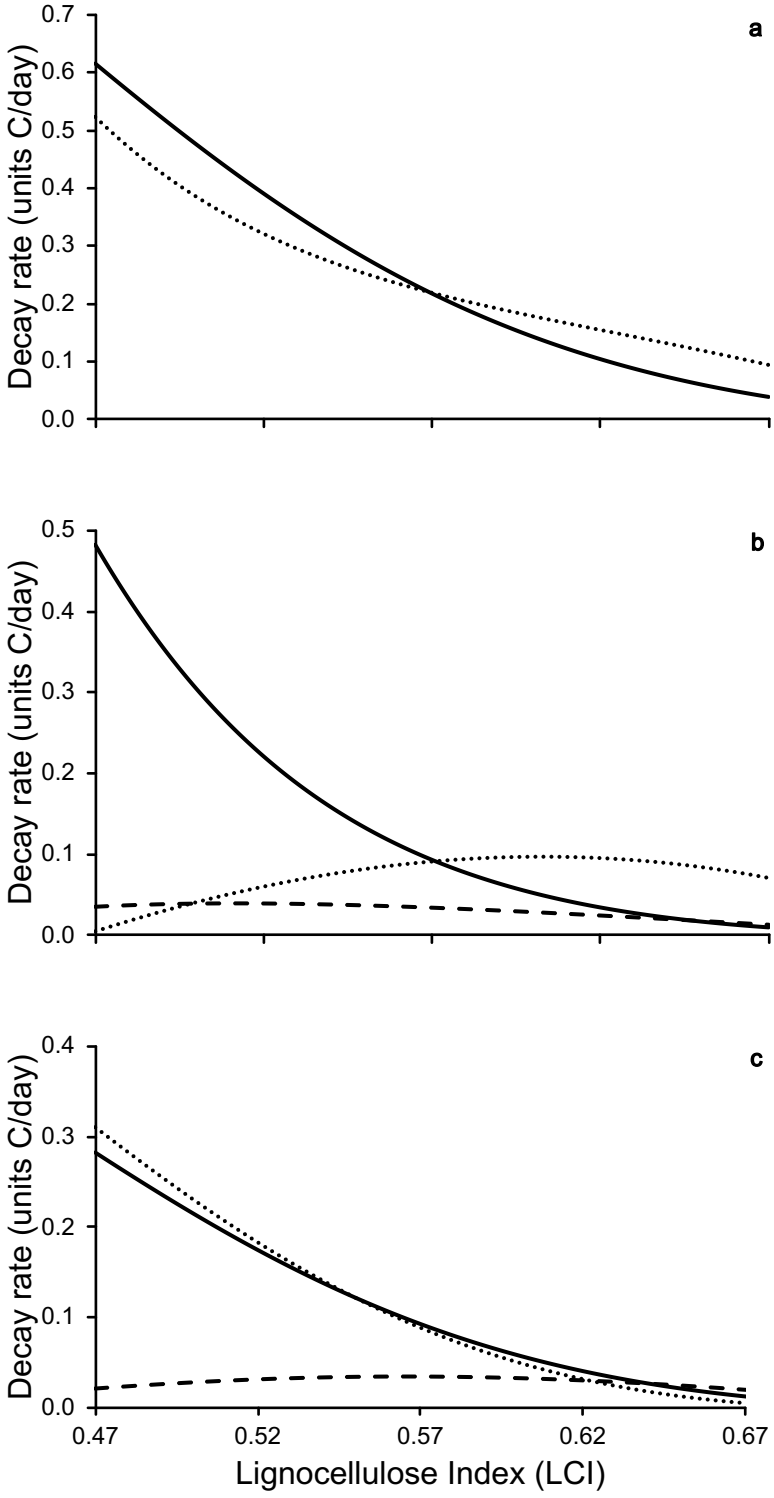

Fig. 2-3: a. Relationships between overall litter decay rate (dC_i/dt) and lignocellulose index (LCI) of litter needed to balance microbial C:N stoichiometry (solid line) and driven by empirically-observed enzyme activities (dotted line); b. Relationships between simulated decay rates for pools of organic nitrogen (dC_1/dt; dotted line),

cellulose (dC_2/dt; solid line), and lignin (dC_3/dt; dashed line) substrates and lignocellulose index (LCI) of litter needed to balance microbial C:N stoichiometry; and c. Relationships between simulated decay rates for pools of organic nitrogen (dC_1/dt; dotted line), cellulose (dC_2/dt; solid line), and lignin (dC_3/dt; dashed line) substrates and lignocellulose index (LCI) of litter driven by empirically-observed enzyme activities.

By definition, C and N fluxes estimated by our stoichiometric balanced model exactly met microbial C and N demands such that estimates of both R_O and N_M remained zero at all LCI. In contrast, simulations driven by the observed values of $alpha_1$ generated excess C and N fluxes beyond what was necessary to exactly balance microbial C and N demand; both decreased with increasing LCI (Fig. 2-4).

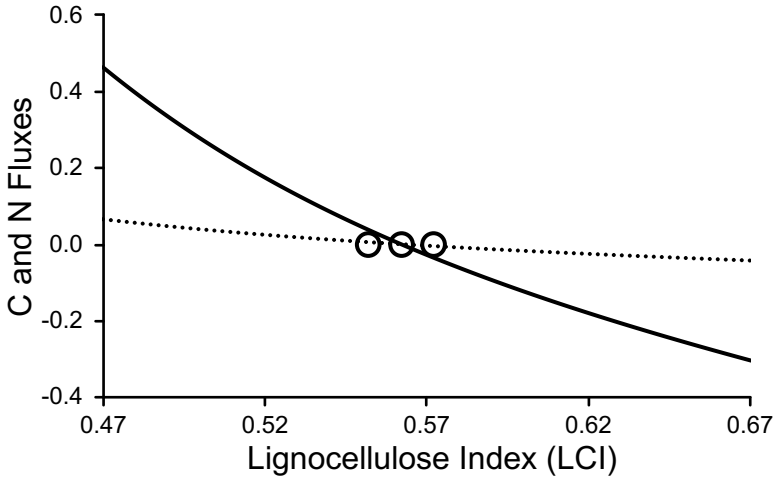

Fig. 2-4: Simulated relationships between calculated nitrogen (dotted line) and carbon (solid line) fluxes needed to balance microbial C:N stoichiometry at given values of lignocellulose index (LCI) of litter; the intersection of C and N fluxes estimates TER = 0.56 at a baseline CN_1 = 7.0 (middle circle), while the other circles show estimated TER = 0.55 and 0.57 with CN_1 at 6.3 and 7.7 (lowest and highest circles, respectively).

The intersection of R_O with N_M defines TER, which occurred at LCI = 0.564 with baseline parameter values (Table 2.2). However, TER varied as parameters affecting the stoichiometric balance between substrate, enzymes and biomass varied. For example, the

three circles shown in figure 4 illustrate increasing TER with increasing C:N ratio of the C_1 pool (CN_1). Moreover, balancing C and N fluxes with microbial stoichiometry at LCI < TER for baseline parameters generated 3.57 g C of cumulative overflow respiration (C mineralization), which would otherwise require 0.50 g of additional nitrogen immobilization to assimilate into microbial biomass. For values of LCI > TER, a subsidy of 9.95 g C would be required for microorganisms to assimilate 1.39 g of N that was mineralized.

2.3.3 Sensitivity analysis

Mean cumulative decomposition was 46.07 ± 3.76% of the original litter mass in sensitivity analyses. Results indicated that LCI_{MID} and EXP accounted for nearly all the explained variation in total substrate decay, with LCI_{MID} , alone, representing over 98% (Table 2.3). The mean value of TER was LCI = 0.484 ± 0.002 in sensitivity analyses and CN_1, CUE_2, LCI_{MID}, and EXP together accounted for about 90% of the variation. LCI_{MID}, alone, accounted for over 62% of the variation in TER.

Table 2.3: Results of ANOVA evaluating sensitivity analysis results (see section 2.3.3); proportional allocation of Type 3 partial sums of squares of ANOVA.

	Source	TER	Decay	Overflow Respiration	Nitrogen Mineralization
Proportion	CN_1	0.121	0.000	0.101	0.565
	CUE_2	0.133	0.000	0.404	0.004
	EXP	0.022	0.019	0.019	0.186
	LCI_{MID}	0.624	0.987	0.434	0.228
	Error	0.074	0.000	0.013	0.017

Variations in C and N fluxes (R_O and N_M) necessarily balance each other because they are generated with respect to stoichiometric requirements of microbial biomass. Thus, results of sensitivity analyses were identical for C and N fluxes. For this reason, we report R_O (C mineralization) when LCI < TER and N_M (N mineralization) when LCI > TER. The mean value of cumulative Ro was 0.394 ± 0.387% of the original litter C mass and CN_1, CUE_2, LCI_{MID}, and EXP together accounted for about 96% of this variation ($R^2 = 0.998$, all $p < 0.01$), whereas the mean value of N_M was 0.155 ± 0.347% of the original litter C mass and CN_1, LCI_{MID}, and EXP explained nearly 99% of this variation ($R^2 = 0.984$, all $p < 0.01$). Both CUE_2 and LCI_{MID} each accounted for over 40% of the variation in cumulative Ro; whereas CN_1 alone accounted for nearly 57% of the variation in cumulative N_M.

2.3.4 Carbon use efficiency

Our stoichiometric balanced model generated a realized CUE for the assimilation of all substrates combined (CUE_T) that decreased by 73% from 0.475 at LCI = 0.47 to 0.127 at LCI = 0.67 (Fig. 2-5). In contrast, CUE_T from simulations driven by observed $alpha_1$ values declined by 36%, from 0.540 at LCI = 0.47 to a minimum of 0.324 at LCI = 0.67. In both models, the carbon use efficiency for the combined lignocellulose pool (CUE_{23}) decreased from 0.45 to 0.07, as LCI increased from 0.47 to 0.67 (Fig. 2-5). Thus, the difference between our stoichiometric model and output generated by the observed values of $alpha_1$ was least at intermediate LCI values. Essentially, this implies that the realized CUE_T driven by empirical observations is higher than the theoretical value balancing microbial stoichiometry at both low and high values of LCI. For comparison, estimates of CUE based on the EEST relationships among biomass, enzymes and substrate characteristics ($CUE_{C:N}$; Eq. 2.10) decreased by 57% from 0.21 at LCI = 0.475 to 0.09 at LCI = 0.67 based on $alpha_1$ from our stoichiometric model. When observed values of $alpha_1$ were used in calculations, $CUE_{C:N}$ increased steeply, from 0.005 at LCI = 0.47 to 0.448 at LCI = 0.67.

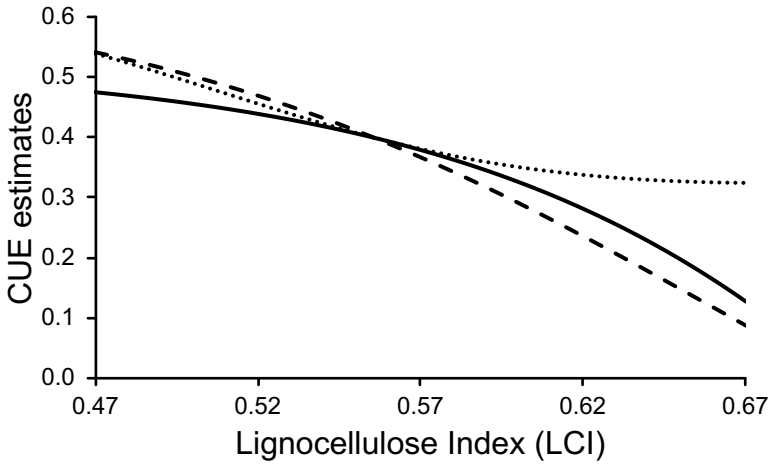

Fig. 2-5: Relationships between realized carbon use efficiency of all substrates combined (CUE_T) and lignocellulose index (LCI) needed to balance microbial C:N requirements (solid line) and driven by empirically-observed enzyme activities (dotted line), and between carbon use efficiency of the lignocellulose pool (CUE_{23}) and LCI (dashed line).

2.4 Discussion

2.4.1 Patterns of litter decay

The allocations of C_1, C_2 and C_3 used in our simulations (Aber et al. 1984, Melillo et al. 1982, Melillo et al. 1989, Magill and Aber 1998, Herman et al. 2008) followed patterns during progressive decomposition consistent with the general conceptual model of leaf litter decay, i.e., cellulose decreased relative to lignin whereas organic nitrogen compounds increased (Berg and McClaugherty 2008, Soong et al. 2019). Interestingly, the rate of decline in relative cellulose concentration was roughly twice the rate of increase in relative organic N concentration. However, the observed patterns of enzyme activities from empirical studies (Snajdr et al. 2011, Carreiro et al. 2000) differed from expectations, based on anticipated decay rates exactly meeting stoichiometric needs of microorganisms (Sinsabaugh and Follstad Shaw 2012) or maximizing microbial growth.

In particular, our stoichiometric model predicted a decrease in $alpha_1$ with LCI, whereas the observed values of $alpha_1$ increased with LCI. Our growth-maximizing model also predicted an increase in $alpha_1$ with LCI but to the exclusive catalysis of the organic N pool by LCI = 0.51. This extreme sensitivity to factors controlling energy and nutrient balance could not be constrained by altering any single parameter, e.g., CN_1, CUE_2, CN_M, etc. (cf. Manzoni et al. 2021). Thus, we focused our attention on the contrast between stoichiometric and empirical models of $alpha_1$.

The novel aspect of our model as driven by both stoichiometric estimates and empirical patterns of enzyme allocation ($alpha_1$) is in making comparisons of stochiometric theory with observations of enzyme activity given the availabilities of the substrates they target (Fig. 2-1). There was no guarantee that resulting patterns of enzyme-driven decomposition rates (e.g., dC_1/dt, dC_2/dt, dC_3/dt) would be consistent with expectations given either allocation scheme. However, the first-order decay rates used in this study are within the range of values commonly reported from empirical descriptions of litter decay and thus likely to force estimates of lignocellulose decay to conform (Parton et al. 1987, Schimel and Weintraub 2003, Moorhead et al. 2014). Indeed, relative rates of cellulose decay (dC_2/dt) declined and lignin decay (dC_3/dt) increased as LCI increased (Fig. 2-2) in both simulations, as the relative amount of C_2 declined with respect to C_3. However, the empirical model had an overall decay rate (dC_T/dt) about 16% lower than the stoichiometric model at LCI = 0.47 with a concomitant lignocellulose decay rate (dC_{23}/dt) that was over 37% higher. The reason for these differences was the rationale for allocating a finite pool of enzymes that was assumed to be a constant fraction (0.4%) of total substrate C. The low value of observed

$alpha_1$ at low LCI allocated more of the total enzyme activity to lignocellulose decay than the stoichiometric model. However, the decay rate for C_3 is lower than C_1 or C_2, reducing the rate of total litter decay per unit enzyme. The relative differences between the two models were reversed at high LCI. The stoichiometric model had an overall decay rate about 60% lower and a lignocellulose decay rate that was about 44% higher than the empirical model at LCI = 0.67. At this point, the empirical model allocated less of the total enzyme pool to lignocellulose decay, which reduced overall decomposition.

The most obvious difference between the two models was in the dynamics of the organic N pool. The observed values of $alpha_1$ increased throughout decomposition whereas the values estimated by the stoichiometric model decreased, driving differences in decay rates. The empirical model had a dC_1/dt that was less than 2% of the estimate for the stoichiometric model at LCI=0.47, but this pattern reversed at LCI=0.67, when the rate for the stoichiometric model was less than 7% of the empirical model. Again, differences in enzyme allocation patterns between the models were responsible for the differences in patterns of substrate turnover. The reasons why these patterns differed are not so obvious. It is possible that other sources of N were available to support microbial needs at low LCI that did not require enzyme activity, such as mineral N or amino acids (Berg and McClaugherty 2008). Regardless, the higher values of dC_1/dt for the empirical model at higher LCI values suggest that microbes use the C_1 fraction as a C source as the composite litter becomes increasingly recalcitrant, mineralizing excess N, consistent with an energy maximizing strategy (Averill 2014). In brief, when microbes are C-limited, they may maximize growth by adjusting enzyme allocation to optimize C gain. Thus, enzyme stoichiometry does not necessarily indicate growth-limiting nutrients because

microbes can utilize N-acquiring enzymes (e.g., NAG and LAP) to gain C as well as N (Hu et al. 2018, Soong et al. 2019, Mori 2020). Of course, it is also possible that an external source of C was available to microorganisms, stimulating catalysis of the N-containing pool to acquire N, i.e., a priming effect (Kuzyakov 2010). Unfortunately, we had no information to estimate the availability of external sources of N or C to the synthetic data set used in this study.

2.4.2 Patterns of enzyme activities

Traditional models of lignocellulose decay (Parton et al. 1987, Berg and McClaugherty 2008, Adair et al. 2008), predict the rapid loss of the readily accessible cellulose fraction early in decomposition, which triggers the onset of lignin decay and slows the overall decay rate. This pattern logically requires a higher allocation of cellulolytic versus ligninolytic enzymes at the start of decomposition that declines with progressive decay, because the presence of recalcitrant C has a negative effect on the decomposition of hydrolysable C (Moorhead et al. 2013, Margida et al. 2020, Manzoni et al. 2021). Both of our models simulated this pattern in the same manner, allocating cellulolytic and ligninolytic enzymes as functions of LCI according to Margida et al. (2020). Differences in rates of overall decomposition (dC_T/dt) and lignocellulose decay (dC_{23}/dt) between these models resulted from differences in the relative allocation of N-acquiring vs. C-acquiring enzymes ($alpha_1$) from a restricted pool of total enzymes. Although the stoichiometric model provided a precise balance of microbial C and N demands, observed allocations did not follow this pattern. Thus, the substrate recalcitrance model of Margida et al. (2020) accurately represented the enzyme-mediated decomposition

of the lignocellulose pool. However, the stoichiometric model of Moorhead et al. (2012) estimated C- and N-acquiring enzyme activities to balance microbial C and N demands without considering a potential switch in strategy to maximize C-acquisition, triggered by a transition from a N-limited to C-limited state (Averill 2014, Mori 2020).

This shift in enzyme allocation strategy also reflects shifts in patterns of relative resource availability including both the sizes and recalcitrance of substrate pools (Sinsabaugh and Follstad Shah 2011, 2012). The amount of enzyme allocated to catalyze a particular substrate tends to be minimized because enzymes are expensive to build and given the kinetics of these reactions, the return on that investment declines rapidly with increasing allocation (Bar-Even 2011). However, that return is also influenced by the relative demands for different resources, such as C and N, which are non-substitutable. This is the basis of the Ecoenzymatic Stoichiometric Theory (EEST; Sinsabaugh and Follstad Shah 2012) and the rationale supporting the stoichiometric model by Moorhead et al. (2012). However, the source of C is substitutable, with N-containing organic compounds also containing considerable C. For example, recent studies (Mori 2020, Norman et al. 2020) showed that microorganisms used aminopeptidase enzymes (e.g., LAP) to acquire C to meet energy demands, and that the amino sugar glucosamine was a source of both N and C to microorganisms (Hu et al. 2018). Furthermore, LAP activities are not always closely related to gross protein depolymerization (Wild et al. 2019); thus, enzyme stoichiometry is not overall a precise indicator of growth-limiting nutrients in soils (Rosinger et al. 2019). The increasing N concentration in decaying litter used in our simulations suggested an increasing pool of organic N compounds (C_1) with progressive decomposition. We assumed that this pool had a consistent, overall C:N ratio of about 7:1.

Thus, the increase in N content implied an increase in related C content that could be accessed by LAP+NAG in our models. The observed linear increases in both litter N concentration and $alpha_1$ with LCI are consistent with this notion. Even so, the C_1 pool in these models never represented more than 17% of the total litter mass (at LCI = 0.67), limiting the potential yield of carbon and thus relative allocation of enzymes ($alpha_1$).

Alternative explanations for differences between the enzyme allocation strategies for our models include microbial access to resources that don't require enzyme activity, such as forms of mineral N and amino acids. Such N sources could reduce the need for N-acquiring enzymes and increase allocation of enzymes for C-acquisition, which might explain the low initial values of observed $alpha_1$ (above). In comparison, Manzoni et al. (2021) posited four alternative resource use modes under N-limiting conditions to fit model predictions to observed patterns of litter decomposition: (1) flexible CUE, (2) reduced synthesis of C-acquiring enzymes, (3) adjustment of microbial C-N requirements to decrease N demand, or (4) assuming microbial N-retention at senescence by increasing N-use efficiency. They were able to approximate observed patterns of decomposition by independently varying each of these controls, generating an equifinality obstacle to selecting any single control. In contrast, we could not match observed patterns of $alpha_1$ by varying any single model parameter affecting C and/or N fluxes, although varying several of them simultaneously could approximate observations (CUE_1, CUE_2, CN_1, CN_M, k_{1max}, etc., not shown). Although it is likely that many of these parameters are in fact adaptive characteristics of a microbial community to changing resource availability, we could find no comprehensive study of tradeoffs between characteristics during long-term decomposition. Regardless, the relative acquisition of C indicated by such low values of

observed $alpha_1$ at low LCI suggests an excess release above the amount that could be assimilated into microbial biomass, especially with the relatively generous values of carbon use efficiencies (CUE) we assumed for both C_1 and C_2. Of course, we also assumed a nitrogen use efficiency (NUE) of 100%, which exacerbated the excess C balance (see Manzoni et al. 2021). This excess C could be lost through overflow metabolism, or slip respiration (Schimel and Weintraub 2003, Soong et al. 2019), when C and N acquisition from substrates fall below the threshold element ratio (TER), and N mineralization when TER is exceeded (below). Thus, the stoichiometry of substrates, enzymes and microbial biomass seems to be not as closely linked as our stoichiometric model simulated. This difference is consistent with reports from other recent studies (Rosinger et al. 2019, Soong et al. 2019, Mori 2020).

2.4.3 Coupled C and N fluxes

Although unexpected, the imbalance between C and N fluxes driven by observed values of $alpha_1$ generated a pattern of C and N mineralization that is also consistent with general models of litter decay (Berg and McClaugherty 2008, Soong et al. 2019). Microbes appear to be meeting their stoichiometric needs through the mineralization of excess C or N, rather than acquiring resources in exact proportion to stoichiometric requirements. The reasons for these imbalances are not entirely clear. The more obvious is that net N mineralization occurs when litter is more recalcitrant (higher LCI) suggesting that microbes are releasing more N than needed to meet stoichiometric demands. This pattern supports Averill's (2014) finding that microbes adopt an energy maximizing strategy at higher LCI values, utilizing N-acquiring enzymes such as NAG

and LAP to mine carbon from the C_1 pool and mineralizing excess N (Rosinger et al. 2019, Norman et al. 2020, Mori 2020). This strategy becomes increasingly cost-effective as the realized CUE for lignocellulose declines and the pool of C_1 increases.

The rationale for overflow metabolism is less clear than N mineralization. Excess C mineralization (R_O) is highest early in decay, when litter is more labile and potential CUE is high, implying that microbes are acquiring more C than needed for growth and maintenance. The purpose of overflow metabolism is thought to overcome stoichiometric imbalance (Manzoni et al. 2012, Soong et al. 2019). Its occurrence implies that C and N acquisition of microorganisms is unbalanced, as indicated by $alpha_1$, although the acquisition of mineral N to supplement microbial nutrition would belie this idea (see above). However, simulated overflow respiration from the empirical model (R_O) is consistent with previous reports of this phenomenon (Zak et al. 1994, Schimel and Weintraub 2003, Moorhead and Sinsabaugh 2006, Cleveland and Liptzin 2007, Colman and Schimel 2013, Xu et al. 2013), indicating that decomposition may be consistently overloaded with C early in decay, and that overflow respiration is an important C flux (Manzoni et al 2012).

2.4.4 Sensitivity analysis

The threshold element ratio (TER) is traditionally expressed as the microbial biomass C:N ratio divided by carbon use efficiency (Frost et al. 2006, Soong et al. 2019). However, that calculation assumes constant substrate and microbial biomass stoichiometry and constant resource assimilation efficiencies (both N and C) throughout decomposition. To the contrary, substrate stoichiometry clearly changes during decay and

overall CUE varies both with substrate stoichiometry (Moorhead et al. 2012, Geyer et al. 2016, Hagerty et al. 2018, Geyer et al. 2019) and LCI (Moorhead et al. 2013, Sinsabaugh et al. 2013, Margida et al. 2020). In this model, we approximated TER as the intersection of overflow respiration (R_O) and (N_M), which occurs only when both values are zero. This method of estimating TER allows for a dynamic estimate of realized CUE_T that changes as decay progresses, and TER estimates varied as expected during decay.

Altering CN_1, CUE_2, EXP, and LCI_{MID} changed the threshold element ratio although patterns of overflow respiration (R_O) and nitrogen mineralization (N_M) remained similar among all simulations. Indeed, the impacts of variations in model parameters on model behavior were largely predictable. Increasing CN_1 or CUE_2 simply increased the amount of C relative to N per unit of substrate decay, increasing the LCI value at which TER occurred as predicted by the simplest estimates of TER (Frost et al. 2006). Increasing LCI_{MID} had the same effect as increasing CUE_2. Increasing the exponent for the half-saturation coefficient (EXP) of enzymes operating on substrate also increased TER. This is because increasing EXP increased the overall impact of enzyme activity per unit of enzyme. This effect was especially notable for N acquisition due to greater proportional allocation to the E_2 and E_3 pools than to the E_1 pool and also because the C_1 pool is much smaller than the C_2 and C_3 pools.

Overall, CUE_2 and CN_1 were the most important controls on R_O, while CN_1 and LCI_{MID} were the most important controls on N_M. When CUE_2 and CN_1 change, the amount of C released also changes, driving an adjustment in R_O. Similarly, when CN_1 and LCI_{MID} change, the amount of N released also changes, driving an adjustment to rates of N_M. In summary, variations in parameters that increased C-acquisition relative to N

increased realized TER and cumulative R_O and decreased cumulative N_M. This was the result of altering realized CUE_T for the aggregated decay of C_1, C_2 and C_3, because the assimilation efficiency for N was assumed to be a constant 100%.

2.4.5 Carbon use efficiency

Tradeoffs in the overall carbon use efficiency (CUE_T) and litter quality during substrate decay may explain the observed increase in $alpha_1$ with increasingly recalcitrant litter. The realized CUE_T for the combined decomposition of all substrates cannot be a constant, as generally assumed in decomposition models (Schimel and Weintraub 2003, Moorhead et al. 2012, Abramoff et al. 2017) with exceptions, such as estimating CUE as a function of temperature (Allison et al. 2010, Wang et al. 2013, Wieder et al. 2015) or estimating CUE from the decay of multiple substrates each with a particular, constant CUE (e.g., Parton et al. 1987). As decay progresses, CUE_{23} decreases, while CUE_1 remains the same in our simulations, making C_1 an increasingly more energy-efficient source of carbon. Additionally, since CUE_T is not fixed, the TER cannot be accurately predicted using the Frost et al. (2006) equation. Alternatively, Sinsabaugh et al. (2016) estimated CUE stoichiometrically ($CUE_{C:N}$) as a function of labile resource availability (both C and N; Eq. 2.10). Surprisingly, estimated $CUE_{C:N}$ declined with LCI for our stoichiometric model and increased with LCI for the empirical model. This was due to the relationship between $alpha_1$ and LCI (appendix A). Clearly, defining a functional CUE is complex (e.g., Geyer et al. 2019). Nonetheless, we found that the stoichiometry of substrate, enzyme activities, and microbial biomass were linked through resource use efficiencies as well as the relative

availabilities of these resources. Those linkages varied more than anticipated due to shifting microbial resource acquisition strategies beyond meeting stoichiometric demands (above).

A key question resulting from these simulations is the value of CUE_{23} at high LCI. Moorhead et al. (2013) assumed this value to be zero at LCI = 0.7, but the observed data (Carreiro et al. 2002, Snajdr et al. 2011) suggest that CUE_{23} is nonzero at this threshold if microbial stoichiometric balance is met by C and N-acquisition through enzyme activities, because observed lignocellulolytic enzymes (E_{23}) account for about 60% of total enzyme activity ($alpha_1$) at that point. We suspect that microbes are mining carbon from the C_1 litter fraction to maximize C acquisition and mineralize excess N (Averill 2014, Soong et al. 2019). We also speculate that CUE_1 declines with LCI because an increasing fraction of total litter N may be bound with the C_{23} fraction as reported by Aber et al. (1984), i.e., in the Van Soest acid insoluble fraction of total litter N (not shown). Generally, the C:N ratio of litter decreases with progressive decay due to the release of C through microbial respiration, while N persists due to immobilization and possibly condensation reactions (Melillo et al. 1982, Preston et al. 2009, Rillig et al. 2007). Changes in the types of organic N substrates during progressive decomposition may alter the relative availability of both the associated C and N. Alternatively, microbes may be mining N from the C_1 litter fraction that is bound with the C_{23} fraction, given an external C supply (priming effect; Kuzyakov 2010). Unfortunately, we cannot test these notions with the existing data.

2.4.6 Limitations and future directions

Perhaps the most obvious limitation of the current work is the uncertainty associated with using a largely synthetic dataset (section 2.1). Ideally, more comprehensive studies that include detailed litter quality, stoichiometry, and eco-enzymatic data would increase the realism, as well as rigor to more conclusively test different hypotheses of microbial resource acquisition in our model. Recent meta-analyses of enzyme activities emphasize soils rather than litter (e.g., Chen 2018, 2020), including the foundational work supporting development of the EEST (Sinsabaugh et al., 2008, 2009, Sinsabaugh and Follstad Shah 2012). Litter studies including enzyme activities tend to be short term and/or lack detailed litter chemistry, including Carriero et al. (2000) and Sinsabaugh and Carriero (2002) used herein. Although the work by Snajdr et al. (2011) provided both, it's a rare example. In contrast, studies including detailed litter chemistry seldom include enzyme activities (Aber et al. 1984, Berg et al. 1991, Magill and Aber 1998, Trofymow et al. 2002, Harmon et al. 2009). We combined different studies by linking mass loss with lignocellulose index, and in turn LCI with detailed litter chemistry and enzyme activities. Although these patterns appeared consistent, they must be interpreted with caution.

There remains much work to link substrate, enzyme and microbial dynamics during decomposition. Other studies have also reported apparent disconnects from EEA and microbial resource demands (e.g., Rosinger et al. 2019, Mori 2020) but syntheses of microbial responses to stoichiometric constraints suggest considerable flexibility in patterns of resource use (Mooshammer et al. 2014, Zechmeister-Boltenstern et al. 2015). In particular, the maximum growth model (Averill 2014) merits further examination

given the recent modeling analysis of Manzoni et al. (2021) demonstrating the plausibility of varying resource use to link microbial processes to patterns of decomposition. However, rigorously testing such a model requires detailed microbial characteristics in addition to the need for concurrent litter chemistry and EEA observations. Again, Snajdr et al. (2011) is an exceptional study that includes all these measures, although the data consist of only eight observations of EEA and microbial characteristics over two years. It represents a demanding study plan, but results are more tantalizing than definitive. Thus, more comprehensive models may necessarily remain largely theoretical until more detailed data are available.

2.5 Conclusions

In conclusion, although evidence, theory, and literature offer potential explanations, we could not isolate the specific reasons why we found essentially opposite patterns between stoichiometric balance and observed values of EEA. Unfortunately, we have no data to definitively support any one explanation. Bradford et al. (2021) states that including microbial-based responses into broad patterns of soil carbon dynamics requires thoroughly understanding underlying processes, because aggregation methods needed to simplify complex processes for inclusion in broad-scale models can obscure important fine-scale responses. For example, aggregating the varying stoichiometric, microbial, and litter quality characteristics of litter decay likely contributes to the equifinality challenge of identifying primary controls given high model complexity and low data availability (Marschmann et al. 2019). Manzoni et al. (2021) encourages modelers to more closely examine the mechanisms underlying decay in order to avoid this problem, but although

we looked at decomposition on a finer scale we were still unable to resolve this limitation. Bradford et al. (2021) suggested addressing this problem through improved empirical data collection processes, which should occur over the long-term and at multiple scales. We heartily concur with this suggestion.

References

Aber, J. D., McClaugherty, C. A., & Melillo, J. M., 1984. Litter decomposition in Wisconsin forests.

Abramoff, R. Z., Davidson, E. A., & Finzi, A. C., 2017. A parsimonious modular approach to building a mechanistic belowground carbon and nitrogen model. Journal of Geophysical Research: Biogeosciences 122, 2418-2434.

Abramoff, R. Z., Xu, X., Hartman, M., O'Brien, S., Feng, W., Davidson, E. A., Finzi, A. C., Moorhead, D. L., Schimel, J., Torn, M., & Mayes, M. A., 2018. The Millennial model: in search of measurable pools and transformations for modeling soil carbon in the new century. Biogeochemistry 137, 51-71.

Allison, S. D., 2005. Cheaters, diffusion and nutrients constrain decomposition by microbial enzymes in spatially structured environments. Ecology Letters 8, 626-635.

Allison, S. D., LeBauer, D. S., Ofrecio, M. R., Reyes, R., Ta, A. M., & Tran, T. M., 2009. Low levels of nitrogen addition stimulate decomposition by boreal forest fungi. Soil Biology & Biochemistry 41, 293-302

Allison, S. D., Weintraub, M. N., Gartner, T. B., & Waldrop, M. P., 2010. Evolutionary-economic principles as regulators of soil enzyme production and ecosystem function. In Soil enzymology (pp. 229-243). Springer, Berlin, Heidelberg.

Averill, C., 2014. Divergence in plant and microbial allocation strategies explains continental patterns in microbial allocation and biogeochemical fluxes. Ecology letters, 17(10), 1202-1210.

Bach, C. E., Warnock, D. D., Van Horn, D. J., Weintraub, M. N., Sinsabaugh, R. L., Allison, S. D., & German, D. P., 2013. Measuring phenol oxidase and peroxidase activities with pyrogallol, L-DOPA, and ABTS: effect of assay conditions and soil type. Soil Biology & Biochemistry 67, 183-191.

Bar-Even, A., Noor, E., Savir, Y., Liebermeister, W., Davidi, D., Tawfik, D. S., & Milo, R., 2011. The moderately efficient enzyme: evolutionary and physicochemical trends shaping enzyme parameters. Biochemistry, 50(21), 4402-4410.

Bengtsson, F., Rydin, H., & Hájek, T., 2018. Biochemical determinants of litter quality in 15 species of Sphagnum. Plant & Soil 425, 161-176.

Berg, B., Booltink, H., Breymeyer, A., Ewertsson, A., Gallardo, A., Holm, B., Johansson, M., Koivuoja, S., Meentemeyer, V., Nyman, P., Olofsson, J., Pettersson, A., Reurslag, A., Staaf, H., Staaf, I., & Uba, L., 1991. Data on Needle Litter Decomposition and Soil Climate as well as Site Characteristics for Some Coniferous Forest.

Berg, B., & McClaugherty, C., 2008. Decomposition as a process. Plant Litter: Decomposition, Humus Formation, Carbon Sequestration, 11-33.

Berg, B., & Staaf, H., 1980. Decomposition rate and chemical changes of Scots pine needle litter. II. Influence of chemical composition. Ecological Bulletins, 373-390.

Bernstein, L., Bosch, P., Canziani, O., Chen, Z., Christ, R. & Riahi, K., 2008. IPCC, 2007: climate change 2007: synthesis report.

Boerjan, W., Ralph, J., & Baucher, M., 2003. Lignin biosynthesis. Annual Review of Plant Biology 54, 519-546.

Bradford, M.A., Wood, S.A., Addicott, E.T., Fenichel, E.P., Fields, N., González-Rivero, J., Jevon, F.V., Maynard, D.S., Oldfield, E.E., Polussa, A. & Ward, E.B., 2021. Quantifying microbial control of soil organic matter dynamics at macrosystem scales. Biogeochemistry, pp.1-22.

Brinkmann, K., Blaschke, L., & Polle, A., 2002. Comparison of different methods for lignin determination as a basis for calibration of near-infrared reflectance spectroscopy and implications of lignoproteins. Journal of Chemical Ecology 28, 2483-2501.

Burns, R.G., DeForest, J.L., Marxsen, J., Sinsabaugh, R.L., Stronberger, M.E., Wallenstein, M.D., Weintraub, M.N., & Zoppini, A., 2013. Soil enzymes in a changing environment: Current knowledge and future directions. Soil Biology & Biochemistry 58, 216-234.

Campbell, E. E., Parton, W. J., Soong, J. L., Paustian, K., Hobbs, N. T., & Cotrufo, M. F., 2016. Using litter chemistry controls on microbial processes to partition litter carbon fluxes with the litter decomposition and leaching (LIDEL) model. Soil Biology & Biochemistry 100, 160-174.

Carreiro, M.M., Sinsabaugh, R.L., Repert, D.A. & Parkhurst, D.F., 2000. Microbial enzyme shifts explain litter decay responses to simulated nitrogen deposition. Ecology 81, 2359–2365.

Chen, J., Luo, Y., García-Palacios, P., Cao, J., Dacal, M., Zhou, X., Li, J., Xia, J., Niu, S., Yang, H., & Shelton, S., 2018. Differential responses of carbon-degrading enzyme activities to warming: Implications for soil respiration. Global Change Biology 24, 4816-4826.

Cleveland, C. C., & Liptzin, D., 2007. C: N: P stoichiometry in soil: is there a "Redfield ratio" for the microbial biomass? Biogeochemistry, 85(3), 235-252.

Colman, B. P., & Schimel, J. P., 2013. Drivers of microbial respiration and net N mineralization at the continental scale. Soil Biology and Biochemistry, 60, 65-76.

Cotrufo, M. F., Soong, J. L., Horton, A. J., Campbell, E. E., Haddix, M. L., Wall, D. H., & Parton, W. J., 2015. Formation of soil organic matter via biochemical and physical pathways of litter mass loss. Nature Geoscience 8, 776.

Fatichi, S., Pappas, C., Zscheischler, J., & Leuzinger, S., 2019. Modelling carbon sources and sinks in terrestrial vegetation. New Phytologist, 221(2), 652-668.

Frey, S. D., Ollinger, S., Nadelhoffer, K., Bowden, R., Brzostek, E., Burton, A., Caldwell, B. A., Crow, S., Goodale, C. L., Grandy, A. S., Finzi, A., Kramer, M. G., Lajtha, K., LeMoine, J., Martin, M., McDowell, W. H., Minocha, R., Sadowsky, J. J., Templer, P. H., & Wickings, K., 2014. Chronic nitrogen additions suppress decomposition and sequester soil carbon in temperate forests. Biogeochemistry 121, 305-316.

Frost, P. C., Benstead, J. P., Cross, W. F., Hillebrand, H., Larson, J. H., Xenopoulos, M. A., & Yoshida, T., 2006. Threshold elemental ratios of carbon and phosphorus in aquatic consumers. Ecology Letters, 9(7), 774-779.

Geyer, K. M., Dijkstra, P., Sinsabaugh, R., & Frey, S. D., 2019. Clarifying the interpretation of carbon use efficiency in soil through methods comparison. Soil Biology and Biochemistry, 128, 79-88.

Geyer, K. M., Kyker-Snowman, E., Grandy, A. S., & Frey, S. D., 2016. Microbial carbon use efficiency: accounting for population, community, and ecosystem-scale controls over the fate of metabolized organic matter. Biogeochemistry, 127(2-3), 173-188.

Hagerty, S. B., Allison, S. D., & Schimel, J. P., 2018. Evaluating soil microbial carbon use efficiency explicitly as a function of cellular processes: implications for measurements and models. Biogeochemistry, 140(3), 269-283.

Hammel, K. E., 1997. Fungal degradation of lignin. Driven by nature: plant litter quality and decomposition 33-45. Oxfordshire, UK: Centre for Agriculture and Bioscience International.

Harmon, M. E., W. L. Silver, B. Fasth, H. U. A. Chen, I. C. Burke, W. J. Parton, S. C. Hart, & W. S. Currie, 2009. Long-term patterns of mass loss during the decomposition of leaf and fine root litter: an intersite comparison. Global Change Biology 15:1320-1338.

Herman, J., Moorhead, D., & Berg, B., 2008. The relationship between rates of lignin and cellulose decay in aboveground forest litter. Soil Biology and Biochemistry, 40(10), 2620-2626.

Iyyemperumal, K., & Shi, W., 2008. Soil enzyme activities in two forage systems following application of different rates of swine lagoon effluent or ammonium nitrate. Applied Soil Ecology 38, 128-136.

Kari, J., Olsen, J. P., Jensen, K., Badina, S. F., Krogh, K. B. R. M., Borch, K., & Westh, P., 2019. Sabatier principle for interfacial (heterogeneous) enzyme catalysis. ACS Catalysis 8, 11966-11972.

Kirk, T. K., & Farrell, R. L., 1987. Enzymatic "combustion": the microbial degradation of lignin. Annual Reviews in Microbiology 41, 465-501.

Klemm, D., Heublein, B., Fink, H. P., & Bohn, A., 2005. Cellulose: fascinating biopolymer and sustainable raw material. Angewandte Chemie International Edition 44, 3358-3393.

Klipp, E., Heinrich, R., 1994. Evolutionary optimization of enzyme kinetic parameters; effect of constraints. Journal of Theoretical Biology 17, 309–323.

Kuzyakov, Y., 2010. Priming effects: interactions between living and dead organic matter. Soil Biology and Biochemistry, 42(9), 1363-1371.

Lashermes, G., Gainvors-Claisse, A., Recous, S., & Bertrand, I., 2016. Enzymatic strategies and carbon use efficiency of a litter-decomposing fungus grown on maize leaves, stems, and roots. Frontiers in Microbiology 7, 1315.

Lineweaver, H., & Burk, D., 1934. The determination of enzyme dissociation constants. Journal of the American chemical society, 56(3), 658-666.

Magill, A. H., & Aber, J. D., 1998. Long-term effects of experimental nitrogen additions on foliar litter decay and humus formation in forest ecosystems. Plant and Soil, 203(2), 301-311.

Manzoni, S., Chakrawal, A., Spohn, M., & Lindahl, B., 2021. Modelling microbial adaptations to nutrient limitation during litter decomposition. Frontiers in Forests and Global Change, 4, 64.

Manzoni, S., & Porporato, A., 2009. Soil carbon and nitrogen mineralization: theory and models across scales. Soil Biology and Biochemistry, 41(7), 1355-1379.

Manzoni, S., Taylor, P., Richter, A., Porporato, A., & Ågren, G. I., 2012. Environmental and stoichiometric controls on microbial carbon‐use efficiency in soils. New Phytologist, 196(1), 79-91.

Margida, M. G., Lashermes, G., & Moorhead, D. L., 2020. Estimating relative cellulolytic and ligninolytic enzyme activities as functions of lignin and cellulose content in decomposing plant litter. Soil Biology and Biochemistry, 141, 107689.

Marschmann, G.L., Pagel, H., Kügler, P. & Streck, T., 2019. Equifinality, sloppiness, and emergent structures of mechanistic soil biogeochemical models. Environmental Modelling & Software, 122, p.104518.

Meentemeyer, V., 1978. Macroclimate and lignin control of litter decomposition rates. Ecology, 59(3), 465-472.

Melillo, J. M., Aber, J. D., Linkins, A. E., Ricca, A., Fry, B., & Nadelhoffer, K. J., 1989. Carbon and nitrogen dynamics along the decay continuum: plant litter to soil organic matter. Plant and soil, 115(2), 189-198.

Melillo, J. M., Aber, J. D., & Muratore, J. F., 1982. Nitrogen and lignin control of hardwood leaf litter decomposition dynamics. Ecology, 63(3), 621-626.

Miller, C., 2000. Understanding the carbon-nitrogen ratio. Acres USA, 30(4), 20-1.

Moorhead, D. L., Lashermes, G., & Sinsabaugh, R. L., 2012. A theoretical model of C-and N-acquiring exoenzyme activities, which balances microbial demands during decomposition. Soil Biology and Biochemistry, 53, 133-141.

Moorhead, D. L., Lashermes, G., Sinsabaugh, R. L., & Weintraub, M. N., 2013. Calculating co-metabolic costs of lignin decay and their impacts on carbon use efficiency. Soil Biology and Biochemistry, 66, 17-19.

Moorhead, D. L., & Sinsabaugh, R. L., 2006. A theoretical model of litter decay and microbial interaction. Ecological Monographs, 76(2), 151-174.

Moorhead, D. L., & Weintraub, M. N., 2018. The evolution and application of the reverse Michaelis-Menten equation. Soil Biology and Biochemistry, 125, 261-262.

Mooshammer, M., Wanek, W., Zechmeister-Boltenstern, S. & Richter, A.A., 2014. Stoichiometric imbalances between terrestrial decomposer communities and their resources: mechanisms and implications of microbial adaptations to their resources. Frontiers in microbiology, 5, p.22.

Mori, T., 2020. Does ecoenzymatic stoichiometry really determine microbial nutrient limitations?. Soil Biology and Biochemistry, 146, 107816.

Neumann, M., Ukonmaanaho, L., Johnson, J., Benham, S., Vesterdal, L., Novotný, R., Verstraeten, A., Lundin, L., Thimonier, A., Michopoulos, P. & Hasenauer, H., 2018. Quantifying carbon and nutrient input from litterfall in European forests using field observations and modeling. Global Biogeochemical Cycles, 32(5), pp.784-798.

Norman, J. S., Smercina, D. N., Hileman, J. T., Tiemann, L. K., & Friesen, M. L., 2020. Soil aminopeptidase induction is unaffected by inorganic nitrogen availability. Soil Biology and Biochemistry, 149, 107952.

Parnas, H., 1975. Model for decomposition of organic material by microorganisms. Soil Biology and Biochemistry, 7(2), 161-169.

Parton, W. J., Schimel, D. S., Cole, C. V., & Ojima, D. S., 1987. Analysis of factors controlling soil organic matter levels in Great Plains grasslands. Soil Science Society of America Journal, 51(5), 1173-1179.

Paul, E., 1981. Mineralization and immobilization of soil nitrogen by microorganisms. Ecologicla Bulletin (Stockholm) 33, 179-195.

Preston, C. M., Nault, J. R., & Trofymow, J. A., 2009. Chemical changes during 6 years of decomposition of 11 litters in some Canadian forest sites. Part 2. 13 C abundance, solid-state 13 C NMR spectroscopy and the meaning of "lignin". Ecosystems, 12(7), 1078-1102.

Rillig, M. C., Caldwell, B. A., Wösten, H. A., & Sollins, P., 2007. Role of proteins in soil carbon and nitrogen storage: controls on persistence. Biogeochemistry, 85(1), 25-44.

Rosinger, C., Rousk, J., & Sandén, H., 2019. Can enzymatic stoichiometry be used to determine growth-limiting nutrients for microorganisms?-A critical assessment in two subtropical soils. Soil Biology and Biochemistry, 128, 115-126.

Schimel, J. P., & Weintraub, M. N., 2003. The implications of exoenzyme activity on microbial carbon and nitrogen limitation in soil: a theoretical model. Soil Biology and Biochemistry, 35(4), 549-563.

Šnajdr, J., Cajthaml, T., Valášková, V., Merhautová, V., Petránková, M., Spetz, P., Leppänen, K. & Baldrian, P., 2011. Transformation of Quercus petraea litter: successive changes in litter chemistry are reflected in differential enzyme activity and changes in the microbial community composition. FEMS microbiology ecology, 75(2), pp.291-303.

Sinsabaugh, R. S., 1994. Enzymic analysis of microbial pattern and process. Biology and Fertility of Soils, 17(1), 69-74.

Sinsabaugh, R. L., 2010. Phenol oxidase, peroxidase and organic matter dynamics of soil. Soil Biology & Biochemistry 42, 391-404.

Sinsabaugh, R. L., Antibus, R. K., & Linkins, A. E., 1991. An enzymic approach to the analysis of microbial activity during plant litter decomposition. Agriculture, Ecosystems & Environment, 34(1-4), 43-54.

Sinsabaugh, R. L., Antibus, R. K., Linkins, A. E., McClaugherty, C. A., Rayburn, L., Repert, D., & Weiland, T., 1993. Wood decomposition: nitrogen and phosphorus dynamics in relation to extracellular enzyme activity. Ecology, 74(5), 1586-1593.

Sinsabaugh, R. L., Belnap, J., Findlay, S. G., Shah, J. J. F., Hill, B. H., Kuehn, K. A., Kuske, C. R., Litvak, M. E., Martinez, N. G., Moorhead, D. L., & Warnock, D. D., 2014. Extracellular enzyme kinetics scale with resource availability. Biogeochemistry, 121(2), 287-304.

Sinsabaugh, R. L., Carreiro, M. M., & Repert, D. A., 2002. Allocation of extracellular enzymatic activity in relation to litter composition, N deposition, and mass loss. Biogeochemistry, 60(1), 1-24.

Sinsabaugh, R. L., & Shah, J. J. F., 2011. Ecoenzymatic stoichiometry of recalcitrant organic matter decomposition: the growth rate hypothesis in reverse. Biogeochemistry, 102(1), 31-43.

Sinsabaugh, R. L., & Follstad Shah, J. J., 2012. Ecoenzymatic stoichiometry and ecological theory. Annual Review of Ecology, Evolution, and Systematics, 43, 313-343.

Sinsabaugh, R. L., Lauber, C. L., Weintraub, M. N., Ahmed, B., Allison, S. D., Crenshaw, C., Contosta, A. R., Cusack, D., Frey, S., Gallo, M. E., Gartner, T. B., Hobbie, S. E., Holland, K., Keeler, B. L., Powers, J. S., Stursova, M., Takacs-Vesbach, C., Waldrop, M. P., Wallenstein, M. D., Zak, D. R., & Zeglin, L. H., 2008. Stoichiometry of soil enzyme activity at global scale. Ecology letters, 11(11), 1252-1264.

Sinsabaugh, R. L., & Linkins, A. E., 1990. Enzymic and chemical analysis of particulate organic matter from a boreal river. Freshwater Biology, 23(2), 301-309.

Sinsabaugh, R. L., Manzoni, S., Moorhead, D. L., & Richter, A., 2013. Carbon use efficiency of microbial communities: stoichiometry, methodology and modelling. Ecology letters, 16(7), 930-939.

Sinsabaugh, R. L., Turner, B. L., Talbot, J. M., Waring, B. G., Powers, J. S., Kuske, C. R. & Follstad Shah, J. J., 2016. Stoichiometry of microbial carbon use efficiency in soils. Ecological Monographs, 86(2), 172-189.

Soong, J. L., Fuchslueger, L., Marañon‐Jimenez, S., Torn, M. S., Janssens, I. A., Penuelas, J., & Richter, A., 2020. Microbial carbon limitation: the need for integrating microorganisms into our understanding of ecosystem carbon cycling. Global change biology, 26(4), 1953-1961.

Soong, J. L., Parton, W. J., Calderon, F., Campbell, E. E., & Cotrufo, M. F., 2015. A new conceptual model on the fate and controls of fresh and pyrolized plant litter decomposition. Biogeochemistry 124, 27-44.

Sterner, R. W., & Elser, J. J., 2002. Ecological stoichiometry: the biology of elements from molecules to the biosphere. Princeton University Press.

Su, R., Lohner, R. N., Kuehn, K. A., Sinsabaugh, R., & Neely, R. K., 2007. Microbial dynamics associated with decomposing Typha angustifolia litter in two contrasting Lake Erie coastal wetlands. Aquatic Microbial Ecology, 46(3), 295-307.

Sulman, B.N., Phillips, R.P., Oishi, A.C., Shevliakova, E. & Pacala, S.W., 2014. Microbe-driven turnover offsets mineral-mediated storage of soil carbon under elevated CO_2. Nature Climate Change, 4(12), pp.1099-1102.

Suseela, V., 2019. Potential roles of plant biochemistry in mediating ecosystem responses to warming and drought. In Ecosystem Consequences of Soil Warming (pp. 103-124). Academic Press.

Talbot, J. M., & Treseder, K. K., 2012. Interactions among lignin, cellulose, and nitrogen drive litter chemistry–decay relationships. Ecology 93, 345-354.

Tang, J.Y., 2015. On the relationships between the Michaelis–Menten kinetics, reverse Michaelis–Menten kinetics, equilibrium chemistry approximation kinetics, and quadratic kinetics. Geoscientific Model Development, 8(12), pp.3823-3835.

Todd-Brown, K.E.O., Randerson, J.T., Post, W.M., Hoffman, F.M., Tarnocai, C., Schuur, E.A.G. & Allison, S.D., 2013. Causes of variation in soil carbon simulations from CMIP5 Earth system models and comparison with observations. Biogeosciences, 10(3), pp.1717-1736.

Trofymow, J. A., T. R. Moore, B. Titus, C. Prescott, I. Morrison, M. Siltanen, S. Smith, J. Fyles, R. Wein, C. Camiré, L. Duschene, L. Kozak, M. Kranabetter, & S. Visser, 2002. Rates of litter decomposition over 6 years in Canadian forests: influence of litter quality and climate. Canadian Journal of Forest Research 32:789-804.

Trofymow, J. A., Morley, C. R., Coleman, D. C., & Anderson, R. V., 1983. Mineralization of cellulose in the presence of chitin and assemblages of microflora and fauna in soil. Oecologia, 60(1), 103-110.Vicca, S., Luyssaert, S., Penuelas, J., Campioli, M., Chapin III, F. S., Ciais, P., Heinemeyer, A., Högberg, P., Kutsch, W. L., Law, B. E., Malhi, Y., Papale, D., Piao, S. L., Reichstein, M., Schulze, E. D., & Janssens, I. A., 2012. Fertile forests produce biomass more efficiently. Ecology letters, 15(6), 520-526.

Van Soest, P. J., Robertson, J. B., & Barry, M. C., 2018. Soluble lignin and its relation to klason lignin, acid-detergent lignin, and digestibility of NDF. Ithaca, NY: Cornell University.

Wang, B., & Allison, S. D., 2019. Emergent properties of organic matter decomposition by soil enzymes. Soil Biology and Biochemistry, 136, 107522.

Wang, G., Post, W. M., & Mayes, M. A., 2013. Development of microbial‐enzyme‐mediated decomposition model parameters through steady‐state and dynamic analyses. Ecological Applications, 23(1), 255-272.

Wang, G., Huang, W., Zhou, G., Mayes, M.A. & Zhou, J., 2020. Modeling the processes of soil moisture in regulating microbial and carbon-nitrogen cycling. Journal of Hydrology, 585, p.124777.

Wieder, W. R., Bonan, G. B., & Allison, S. D., 2013. Global soil carbon projections are improved by modelling microbial processes. Nature Climate Change, 3(10), 909-912.

Wieder, W.R., Allison, S.D., Davidson, E.A., Georgiou, K., Hararuk, O., He, Y., Hopkins, F., Luo, Y., Smith, M.J., Sulman, B. & Todd‐Brown, K., 2015. Explicitly representing soil microbial processes in Earth system models. Global Biogeochemical Cycles, 29(10), pp.1782-1800.

Whittinghill, K. A., Currie, W. S., Zak, D. R., Burton, A. J., & Pregitzer, K. S., 2012. Anthropogenic N deposition increases soil C storage by decreasing the extent of litter decay: analysis of field observations with an ecosystem model. Ecosystems, 15(3), 450-461.

Xu, X., Thornton, P. E., & Post, W. M., 2013. A global analysis of soil microbial biomass carbon, nitrogen and phosphorus in terrestrial ecosystems. Global Ecology and Biogeography, 22(6), 737-749.

Zak, J. C., Willig, M. R., Moorhead, D. L., & Wildman, H. G., 1994. Functional diversity of microbial communities: a quantitative approach. Soil Biology and Biochemistry, 26(9), 1101-1108.

Zechmeister-Boltenstern, S., Keiblinger, K.M., Mooshammer, M., Peñuelas, J., Richter, A., Sardans, J. & Wanek, W., 2015. The application of ecological stoichiometry to plant–microbial–soil organic matter transformations. *Ecological Monographs*, *85*(2), pp.133-155.

Appendix A

Chapter 2 Equations

Given Reverse Michaelis Menten (RMM) parameters V_{MAX2+3} and K_{E2+3} of the combined lignocellulose pool, the solution for the proportionality $alpha_1 = E_1 / (E_1 + E_{2+3})$ can be derived from reordering equation 2.1:

$$alpha_1 = ½ \cdot (((CN_1 \cdot CUE_1 - CN_B)^2 \cdot (E_T + K_{E2+3})^2 \cdot V_{MAX1}^2 + 2 \cdot CN_1 \cdot V_{MAX2+3} \cdot (CN_1 \cdot CUE_1 - CN_B) \cdot CUE_{2+3} \cdot (E_T^2 + (K_{E1} + K_{E2+3}) \cdot E_T - K_{E1} \cdot K_{E2+3}) \cdot V_{MAX1} + CN_1^2 \cdot CUE_{2+3}^2 \cdot V_{MAX2+3}^2 \cdot (E_T + K_{E1})^2)^{1/2} + ((CUE_1 \cdot E_T + CUE_1 \cdot K_{E2+3}) \cdot CN_1 - CN_B \cdot E_T - CN_B \cdot K_{E2+3}) \cdot V_{MAX1} + (CUE_{2+3} \cdot E_T \cdot V_{MAX2+3} - CUE_{2+3} \cdot K_{E1} \cdot V_{MAX2+3}) \cdot CN_1) / ((CN_1 \cdot CUE_1 - CN_B) \cdot V_{MAX1} + CN_1 \cdot CUE_{2+3} \cdot V_{MAX2+3}) / E_T$$

The solution for $alpha_1$ allows allocation of $E_{2+3} = (1 - alpha_1) \cdot E_T$, so that the solution for the proportionality $alpha_2 = E_2 / (E_2 + E_3)$ can be derived from reordering equation 2.5:

$$alpha_2 = ½ \cdot ((V_{MAX2} + V_{MAX3} - dC_{2+3}dt) \cdot E_{2+3} + (V_{MAX2} - dC_{2+3}dt) \cdot K_{E3} + (-V_{MAX3} + dC_{2+3}dt) \cdot K_{E2} - ((E_{2+3} + K_{E3})^2 \cdot V_{MAX2}^2 + ((2 \cdot E_{2+3}^2 + (2 \cdot K_{E2} + 2 \cdot K_{E3}) \cdot E_{2+3} - 2 \cdot K_{E3} \cdot K_{E2}) \cdot V_{MAX3} - 2 \cdot dC_{2+3}dt \cdot (E_{2+3} + K_{E3}) \cdot (K_{E2} + K_{E3} + E_{2+3})) \cdot V_{MAX2} + ((K_{E2} + E_{2+3}) \cdot V_{MAX3} - dC_{2+3}dt \cdot (K_{E2} + K_{E3} + E_{2+3}))^2)^{1/2}) / (V_{MAX2} + V_{MAX3} - dC_{2+3}dt) / E_{2+3}$$

Alternatively, microbes may seek to maximize growth (μ) by using the C_1 substrate pool as a primary carbon source and simply mineralizing excess N; conditions generating maximum μ were determined by setting the derivative $d\mu/d(alpha_1)$ to zero and solving for $alpha_1$, which can be done by expanding equation 2.4:

$$alpha_1 = CUE_1 \cdot K_{E1} \cdot V_{MAX1} \cdot E_T + CUE_1 \cdot K_{E1} \cdot K_{E2+3} \cdot V_{MAX1} + CUE_{2+3} \cdot K_{E1} \cdot K_{E2+3} \cdot V_{MAX2+3} - (CUE_1 \cdot CUE_{2+3} \cdot E_T^2 \cdot K_{E1} \cdot K_{E2+3} \cdot V_{MAX1} \cdot V_{MAX2+3} + 2 \cdot CUE_1 \cdot CUE_{2+3} \cdot E_T \cdot K_{E1}^2 \cdot K_{E2+3} \cdot V_{MAX1} \cdot V_{MAX2+3} + 2 \cdot CUE_1 \cdot CUE_{2+3} \cdot E_T \cdot K_{E1} \cdot K_{E2+3}^2 \cdot V_{MAX1} \cdot V_{MAX2+3} + CUE_1 \cdot CUE_{2+3} \cdot K_{E1}^3 \cdot K_{E2+3} \cdot V_{MAX1} \cdot V_{MAX2+3} + 2 \cdot CUE_1 \cdot CUE_{2+3} \cdot K_{E1}^2 \cdot K_{E2+3}^2 \cdot V_{MAX1} \cdot V_{MAX2+3} + CUE_1 \cdot CUE_{2+3} \cdot K_{E1} \cdot K_{E2+3}^3 \cdot V_{MAX1} \cdot V_{MAX2+3})^{1/2}) / (CUE_1 \cdot K_{E1} \cdot V_{MAX1} - CUE_{2+3} \cdot K_{E2+3} \cdot V_{MAX2+3}) / E_T)$$

Given empirical $alpha_1$, overflow metabolism (R_O) was estimated by expanding eqn. 1:

$$R_O = CN_1 \cdot CUE_1 \cdot E_T \cdot V_{MAX1} \cdot alpha_1^2 + CN_1 \cdot CUE_{2+3} \cdot E_T \cdot V_{MAX2+3} \cdot alpha_1^2 - CN_1 \cdot CUE_1 \cdot E_T \cdot V_{MAX1} \cdot alpha_1 - CN_1 \cdot CUE_1 \cdot KME_{2+3} \cdot V_{MAX1} \cdot alpha_1 - CN_1 \cdot CUE_{2+3} \cdot E_T \cdot VMAX_{2+3} \cdot alpha_1 + CN_1 \cdot CUE_{2+3} \cdot K_{ME1} \cdot V_{MAX2+3} \cdot alpha_1 - CN_M \cdot E_T \cdot V_{MAX1} \cdot alpha_1^2 - CN_1 \cdot CUE_{2+3} \cdot K_{ME1} \cdot V_{MAX2+3} + CN_M \cdot E_T \cdot V_{MAX1} \cdot alpha_1 + CN_M \cdot K_{ME2+3} \cdot V_{MAX1} \cdot alpha_1) / (E_T \cdot alpha_1 - E_T - K_{ME2+3}) \cdot E_T / (E_T \cdot alpha_1 + K_{ME1}) / CN_1$$

Similarly, nitrogen immobilization (N_M) was derived:

$$N_M = E_T \cdot (CN_1 \cdot CUE_1 \cdot E_T \cdot V_{MAX1} \cdot alpha_1^2 + CN_1 \cdot CUE_{2+3} \cdot E_T \cdot V_{MAX2+3} \cdot alpha_1^2 - CN_1 \cdot CUE_1 \cdot E_T \cdot V_{MAX1} \cdot alpha_1 - CN_1 \cdot CUE_1 \cdot K_{ME2+3} \cdot V_{MAX1} \cdot alpha_1 - CN_1 \cdot CUE_{2+3} \cdot E_T \cdot V_{MAX2+3} \cdot alpha_1 + CN_1 \cdot CUE_{2+3} \cdot K_{ME1} \cdot V_{MAX2+3} \cdot alpha_1 - CN_M \cdot E_T \cdot V_{MAX1} \cdot alpha_1^2 - CN_1 \cdot CUE_{2+3} \cdot K_{ME1} \cdot V_{MAX2+3} + CN_M \cdot E_T \cdot V_{MAX1} \cdot alpha_1 + CN_M \cdot K_{ME2+3} \cdot$$

$V_{MAX1} \cdot alpha_1) / CN_1 / CN_M / (E_T^2 \cdot alpha_1^2 - E_T^2 \cdot alpha_1 + E_T \cdot K_{ME1} \cdot alpha_1 - E_T \cdot K_{ME2+3} \cdot alpha_1 - E_T \cdot K_{ME1} - K_{ME1} \cdot K_{ME2+3})$